Article

Structure

The Y9P Variant of the Titin I27 Module: Structural Determinants of Its Revisited Nanomechanics

Highlights

- I27Y9P mechanostability is similar to the wild-type and different from that published
- NMR can be fully applied to the high-resolution structural analysis of polyproteins
- NMR studies show that polyproteins may induce structural changes in the monomer
- Structural data from the I27Y9P polyprotein fully explain its nanomechanics

Authors

Javier Oroz, Marta Bruix, Douglas V. Laurents, Albert Galera-Prat, Jörg Schönfelder, Francisco Javier Cañada, Mariano Carrión-Vázquez

Correspondence

mcarrion@cajal.csic.es

In Brief

The polyprotein strategy can alter the structure of the protein domain under study. Oroz et al. prove that NMR spectroscopy is a good method to test this possibility. Using this approach, they show that the titin I27Y9P variant has similar mechanical stability to the wild-type.

Oroz et al., 2016, Structure *24*, 606–616
April 5, 2016
http://dx.doi.org/10.1016/j.str.2016.02.016

CellPress

CellPress

Structure
Article

The Y9P Variant of the Titin I27 Module: Structural Determinants of Its Revisited Nanomechanics

Javier Oroz,[1,2,6] Marta Bruix,[3] Douglas V. Laurents,[3] Albert Galera-Prat,[1,2] Jörg Schönfelder,[4] Francisco Javier Cañada,[5] and Mariano Carrión-Vázquez[1,2,*]

[1]Instituto Cajal, IC-CSIC, Avenida Doctor Arce 37, 28002 Madrid, Spain
[2]Instituto Madrileño de Estudios Avanzados en Nanociencia (IMDEA Nanociencia), Cantoblanco, 28049 Madrid, Spain
[3]Instituto de Química-Física Rocasolano, CSIC, Serrano 119, 28006 Madrid, Spain
[4]Centro Nacional de Biotecnología, CSIC, Darwin, 28049 Madrid, Spain
[5]Chemical and Physical Biology, Centro de Investigaciones Biológicas, CSIC, Ramiro de Maeztu 9, 28040 Madrid, Spain
[6]Present address: German Center for Neurodegenerative Diseases (DZNE) and Department of NMR-Based Structural Biology, Max Planck Institute for Biophysical Chemistry, Am Fassberg 11, 37077 Göttingen, Germany
*Correspondence: mcarrion@cajal.csic.es
http://dx.doi.org/10.1016/j.str.2016.02.016

SUMMARY

The titin I27 module from human cardiac titin has become a standard in protein nanomechanics. A proline-scanning study of its mechanical clamp found three mechanically hypomorphic mutants and a paradoxically hypermorphic mutant (I27Y9P). Both types of mutants have been commonly used as substrates of several protein unfoldase machineries in studies relating protein mechanostability to translocation or degradation rates. Using single-molecule force spectroscopy based on atomic force microscopy, polyprotein engineering, and steered molecular dynamics simulations, we show that, unexpectedly, the mechanostability of the Y9P variant is comparable to the wild type. Furthermore, the NMR analysis of homomeric polyproteins of this variant suggests that these constructs may induce slight structural perturbations in the monomer, which may explain some minor differences in this variant's properties; namely the abolishment of the mechanical unfolding intermediate and a reduced thermal stability. Our results clarify a previously reported paradoxical result in protein nanomechanics and contribute to refining our toolbox for understanding the unfolding mechanism used by translocases and degradation machines.

INTRODUCTION

Mechanical stability is an important biophysical and biological protein property that can only be measured by single-molecule force spectroscopy (SMFS). Since this parameter is not correlated with the thermodynamic stability of a protein, it must be directly measured (Carrión-Vázquez et al., 2000; Paci and Karplus, 2000; Best et al., 2001, 2003; Fowler et al., 2002). This difference is due to the fact that mechanical unfolding is a kinetic process that follows different reaction coordinates than thermal or chemical denaturation. Still, at low force loading rates, the pathways can coincide (Fowler et al., 2002; Williams et al., 2003; Cecconi et al., 2005). Consequently, in order to determine the mechanical stability of a protein, one must directly unfold it by SMFS techniques. In these conditions, several unfolding states that may be masked in bulk can sometimes be readily observed (Carrión-Vázquez et al., 2006).

One of the most frequently used techniques to analyze the mechanical properties of a protein is atomic force microscopy (AFM) in its SMFS mode. In this technique, a series of tandem repeats of protein modules (termed polyproteins) are commonly used as a strategy to identify the unfolding of individual protein molecules (Carrión-Vázquez et al., 2006). An important question is whether this strategy affects the mechanical properties of isolated (i.e., untethered) proteins. Several studies have reported effects (usually stabilization) on the mechanical (Li et al., 2000a) as well as thermal or chemical (Tripp and Barrick, 2004; Batey and Clarke, 2008; Randles et al., 2008) stability of an individual protein or module when they are arranged in tandem in polyproteins. However, since this stabilization effect, usually arising from unspecific interactions between modules or between modules and linkers (Politou et al., 1994, 1996; Scott et al., 2002; Rounsevell et al., 2005), does not alter the module's unfolding pathway, the divide and conquer strategy of dissecting large modular proteins into their individual modules to determine their folding equilibrium is still perfectly valid (Batey and Clarke, 2008). One example of a protein module whose mechanical stability is not affected when linked in a polyprotein is the I27 module from human cardiac titin (Rief et al., 1997; Carrión-Vázquez et al., 1999; Li et al., 2000a; García-Manyes et al., 2007). Indeed, I27 has become a model protein for studies addressing mechanical unfolding processes (Carrión-Vázquez et al., 2006) as well as the thermal or chemical denaturing equilibria (Politou et al., 1994, 1996; Carrión-Vázquez et al., 1999; Fowler and Clarke, 2001; Fowler et al., 2002; Best et al., 2003; Wright et al., 2003).

Titin, the longest known natural polypeptide, is the biological spring responsible for sarcomere passive elasticity (Linke and Grützner, 2008). The extendable region of titin is the so-called I band, which is formed by dozens of immunoglobulin (Ig) modules arranged in tandem. Although there is still some controversy regarding unfolding of these Ig modules under physiological

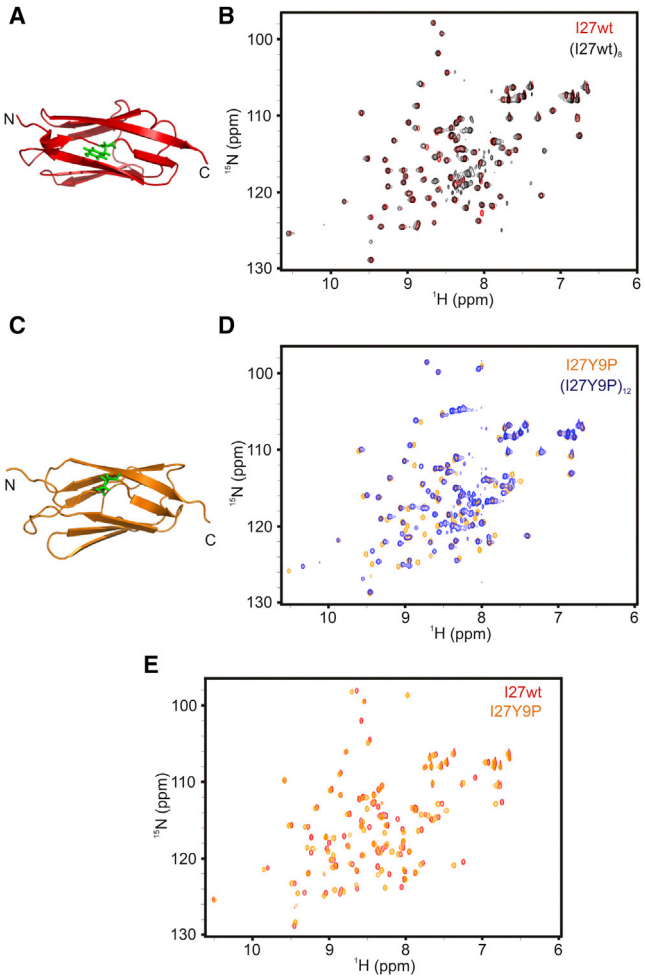

Figure 1. Tertiary Structures and 2D ^{1}H-^{15}N-HSQC Spectra of I27wt and I27Y9P

(A) 3D structure of I27wt (PDB: 1TIT; Improta et al., 1996). Tyr 9 is indicated.

(B) Superposition of the 2D ^{1}H-^{15}N-HSQC spectra of I27wt (red) and $(I27wt)_8$ (black).

(C) 3D structure of I27Y9P (PDB: 2RQ8; Yagawa et al., 2010). Pro 9 is indicated. The molecule is oriented as in (A), showing the molecular clamp close to the C terminus at the front. Relative to I27wt, the N-terminal region of I27Y9P undergoes the largest changes. The figure, like the one shown in (A), was generated using PyMOL (version 1.7; Schrödinger).

(D) Superposition of the 2D ^{1}H-^{15}N-HSQC spectra of I27Y9P (orange) and $(I27Y9P)_{12}$ (blue). Larger δ differences are observed here compared with (B).

(E) Superposition of the 2D ^{1}H-^{15}N-HSQC spectra of I27wt (red) and I27Y9P (orange).

See also Figures 2 and S1.

conditions (Linke et al., 1996; Gautel et al., 1996), several lines of evidence support the idea that some titin Ig modules from the I band, including I27, can unfold under physiological strain and, accordingly, the mechanical unfolding of I27 could be biologically relevant (Linke and Grützner, 2008).

The I27 module (Labeit and Kolmerer, 1995; also called I91 in an updated nomenclature by Bang et al., 2001) contains 89 amino acid residues adopting an Ig β-sandwich fold with seven β strands arranged in two parallel β sheets (Figure 1A). Its mechanical unfolding reveals a metastable intermediate state derived from the rupture of a patch of backbone H bonds between A and B antiparallel β strands (residues 4–7 and 18–25, respectively). This state only appears in mechanical unfolding (Fowler and Clarke, 2001) and is independent of the main determinant of mechanical stability (the mechanical clamp), which is formed by backbone H bonds located between A′ and G parallel β strands (residues 11–15 and 78–87, respectively; Lu et al., 1998; Marszalek et al., 1999; Fowler et al., 2002). However, at low loading rates where unfolding forces are below 43 pN, this intermediate disappears and the module unfolds following a pathway similar to that observed in chemical denaturation (Fowler et al., 2002; Williams et al., 2003). Moreover, it has been established that the module's hydrophobic core does not contribute significantly to the mechanical stability, although it does determine its thermodynamic stability (Best et al., 2003; Stacklies et al., 2009).

Several variants of I27 were designed to examine the structural elements that contribute to its mechanical stability (Li et al., 2000b; Brockwell et al., 2002; Best et al., 2003). One of them, I27Y9P (Figure 1C) unexpectedly showed an increase in its mechanical stability (268 pN versus 204 pN for I27wt; Li et al., 2000b). This was surprising considering that this proline substitution was aimed at impeding the formation of one of the backbone H bonds in the module's mechanical clamp (Lu et al., 1998; Marszalek et al., 1999; Fowler et al., 2002), and therefore a reduced mechanical stability was expected. Interestingly, this variant, together with I27wt and other variants, has been used as a model substrate protein to examine the mechanism of protein unfolding by translocases and protein degradation machines (Kenniston et al., 2003, 2004; Sato et al., 2005; Feng and Lu, 2007; Oguro et al., 2009; Shin et al., 2009; Ruprecht et al., 2010; Yagawa et al., 2010; Cordova et al., 2014). The present study was initially aimed at understanding the structural basis of the surprising mechanical phenotype of I27Y9P reported previously (Li et al., 2000b). However, by performing nuclear magnetic resonance (NMR) spectroscopy analysis of monomeric (I27wt and I27Y9P) as well as polyprotein constructs ($(I27wt)_8$ and $(I27Y9P)_{12}$; Figure 1), in combination with in-depth experimental and simulation analyses of its mechanical unfolding, we show that, contrary to what was reported, the mechanical properties of I27Y9P are very similar to those of I27wt, with minor differences that can be fully explained by subtle structural changes observed in the polyprotein used for the mechanical studies.

RESULTS AND DISCUSSION

I27Y9P Shows Local Structural Perturbations when Tandemly Fused into a Polyprotein

In order to characterize the putative structural changes that could account for the paradoxical mechanical stability reported for I27Y9P (Li et al., 2000b), we performed heteronuclear NMR spectroscopy analysis of monomeric (I27wt and I27Y9P) as well as polyprotein constructs ($(I27wt)_8$ and $(I27Y9P)_{12}$; Figure 1), which are the typical fusion proteins used in SMFS (Carrión-Vázquez et al., 1999). To our knowledge, except for the 2D ^{1}H-^{15}N-heteronuclear single quantum coherence (HSQC) spectra already reported on a $(I27wt)_3$ construct (Best et al., 2001), our work constitutes the first high-resolution structural analysis performed on large polyproteins, whose molecular

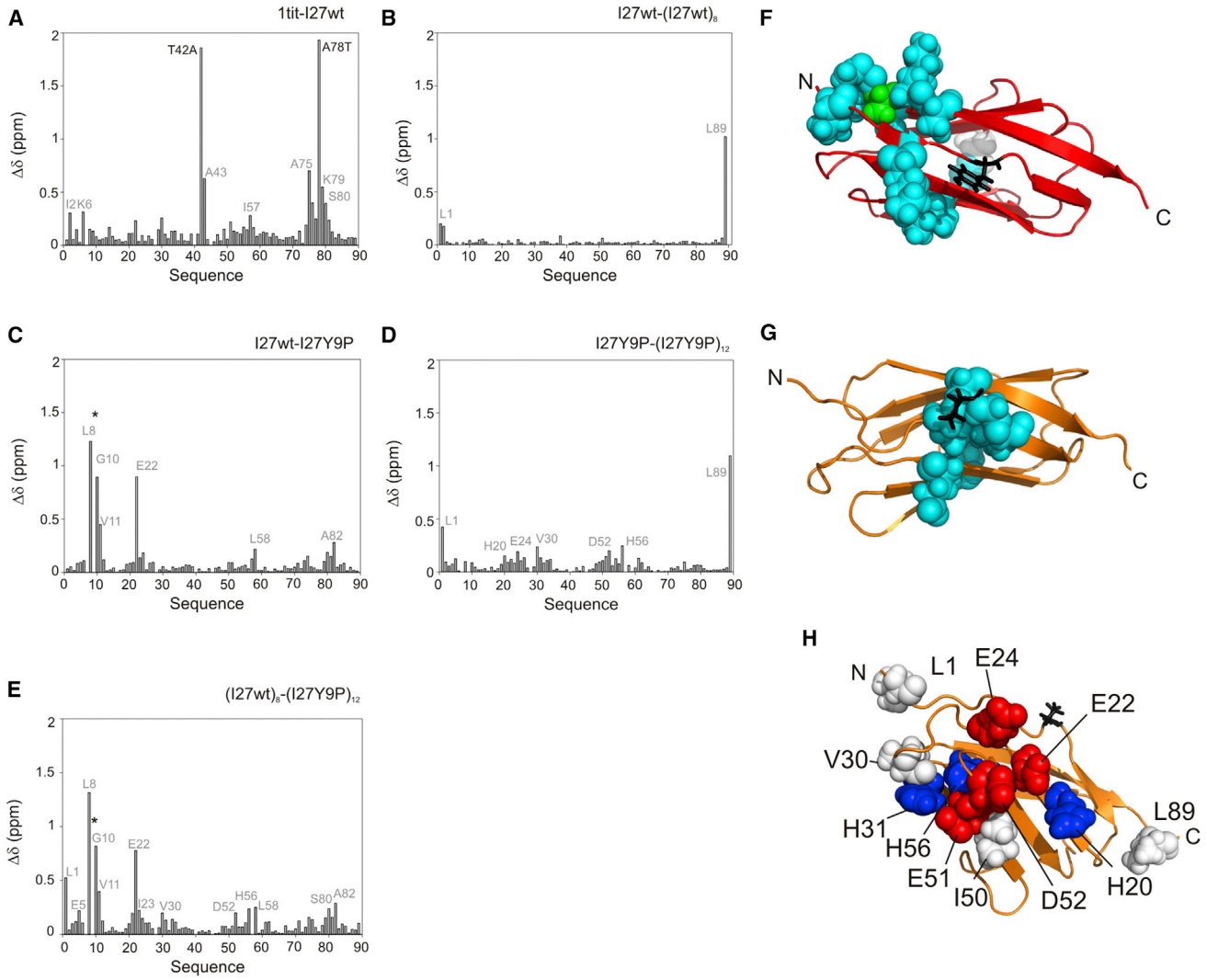

Figure 2. Δδ Analysis of Backbone Amides

(A–E) In (A) the two substitutions compared with the PDB: 1TIT sequence (T42A and A78T) are labeled in black. The asterisk in (C) and (E) indicates the Y9P substitution. Unlike I27wt (B), I27Y9P undergoes subtle structural rearrangements in the polyprotein construct (D). Δδ values were calculated using the equation $[\Delta\delta(^{1}H)^{2} + (\Delta\delta(^{15}N)/5)^{2}]^{1/2}$. The residues with substantial Δδ are indicated in gray (their positions are shown in (F), (G) and (H).

(F) Location of the residues with the largest chemical shift changes (Δδ, cyan spheres) found in I27wt versus PDB: 1TIT (A). These residues are found in the N-terminal region of the protein, in line with what was already proposed for T78A substitution (Stacklies et al., 2009). The atomic structure used was PDB: 1TIT (Improta et al., 1996). We represent T78 in green, whereas A42 is represented in white. Y9 is shown in black sticks representation.

(G) Location of the residues with the largest Δδ (cyan spheres) found in I27 Y9P versus I27wt (C). The structural perturbations caused by the Y9P substitution are very local. As mentioned in the main text, there is spatial connectivity between the residues undergoing the largest Δδ.

(H) The residues showing the largest Δδ in I27 Y9P when arranged in polyprotein (D) form an exposed electrostatic cluster (except H56, which is buried in the core), suggesting possible electrostatic interactions between repeats. The color code used here represents the physicochemical properties of the residue: blue for positively charged, red for negatively charged, and white for hydrophobic. The atomic structure (G and H) used was PDB: 2RQ8 (Yagawa et al., 2010). P9 is shown in stick representation (G and H). The graphs were prepared using PyMOL.

See also Figures S2 and S3.

weights are rather high for this technique ($(I27wt)_8$ is ~80 kDa while $(I27Y9P)_{12}$ is ~120 kDa; Figure S1).

Based on our spectra (Figures 1B, 1D, and 1E), and using the chemical shift (δ) values reported for I27wt (PDB: 1TIT; Improta et al., 1996) as a reference, we assigned most of the ^{1}H and ^{15}N atoms of the residues contained in the different protein constructs (Figure 2). We note that the I27 sequence utilized by Improta et al. (1996) in their original NMR structural study contained Thr at position 42 and Ala at 78, whereas other structural (Stacklies et al., 2009; Yagawa et al., 2010) and most nanomechanical studies (Rief et al., 1997; Carrión-Vázquez et al., 1999; Li et al., 2000b), including the present investigation, use I27 with Ala 42 and Thr 78 as wild-type (Table S1). Both mutations induce large chemical shift changes (Δδ) mainly restricted

to regions near the point substitutions; the overall similarity of the δ values indicates that the global fold is maintained (Figure 2F).

The δ values for I27wt were then compared with those obtained for $(I27wt)_8$ (Figures 1B and 2B) and appear to be identical, except at the termini. This result is expected, as the protein termini are free in I27wt, but connected to a linker between tandem repeats in $(I27wt)_8$. Hence, our results show that I27wt retains its structure when arranged in a polyprotein, in agreement with previous evidence showing that the mechanical stability of the monomer remains identical in the polyprotein (García-Manyes et al., 2007).

We then compared I27wt δ values with those of the I27Y9P mutant, in both monomer (Figures 1E and 2C) and polyprotein (Figure 2E). In the monomer, the perturbations were located in the neighborhood of the substitution site (L8 and G10-V11), in residues spatially close by (E22 and A82), and in a region (L58) whose structure is modulated by E22 and A82 (Figure 2G). We note that the δ values reported here for I27Y9P are in excellent agreement with those reported previously (at higher pH, Table S1; Yagawa et al., 2010). Thus, these data indicate that the structural perturbations produced by the mutation are relatively local.

However, the comparison of NMR data for the I27Y9P monomer and polyprotein showed appreciable alterations (Figures 1D and 2D), larger than those observed in the I27wt constructs. Since the residues showing significant Δδ are in segments that form an exposed electrostatic cluster (Figure 2H), the observed Δδ could be due to unspecific interactions between modules in the polyprotein, an effect that does not seem to perturb I27wt polyproteins (Best et al., 2001) but is present in other I27 variants (Rounsevell et al., 2005). It is interesting to note that the residue in the B β strand that establishes the A-B backbone H patch (E24) shows different δ values with respect to the monomer (see below). Finally, the comparison between I27wt and I27Y9P polyproteins (Figure 2E) reveals changes in similar regions to those observed between the monomers plus the specific perturbations observed in I27Y9P polyprotein. In principle, it is possible that the structural changes in the A-B patch could lead to a mechanical effect on the intermediate state of I27Y9P. Moreover, there was evidence of alterations at the beginning of the A′ strand (L8) as well as in the initial region of the G strand (around S80-A82), which could also alter the mechanical clamp and would therefore explain the previously reported higher mechanical stability for I27Y9P (Li et al., 2000b), since a longer patch of H bonds in the mechanical clamp would account for a higher mechanical stability of the protein (Carrión-Vázquez et al., 2000).

In order to test the possibility of newly formed H bonds in the mechanical clamp of I27Y9P, 3D ^{1}H-^{15}N nuclear Overhauser enhancement spectroscopy (NOESY) experiments were analyzed to resolve long range nuclear Overhauser effects (NOEs) between all the ^{1}H atoms of the residues involved in the mechanical clamps spatially located within 5 Å (Figure S2). In $(I27wt)_8$, the NOEs were strictly comparable with those observed in the monomer, leading us to conclude that the mechanical determinants of $(I27wt)_8$ are the same as those of the I27wt monomer. In particular, our data reveal distances compatible with backbone H bond formation between E5, K6, and E24, which are broken in the mechanical intermediate state (A-B backbone H bond patch; Lu et al., 1998; Marszalek et al., 1999; Fowler et al., 2002); and between Y9, V11, V13, V15 and N83, K85 and K87, constituting the main mechanical clamp of the protein (A′-G patch; Lu et al., 1998; Lu and Schulten, 2000; Li et al., 2000b).

The I27Y9P and I27wt monomers show comparable NOEs both at the mechanical intermediate and in the main mechanical clamp. Interestingly, the NOEs observed in $(I27Y9P)_{12}$ resemble those in I27Y9P except for small differences such as those found between E5 (NH) and L25 ($H\alpha$) and K6 (NH) and E24 (NH), which stabilize the AB patch and are absent in $(I27Y9P)_{12}$ (Figure S2). Therefore, our results indicate that the structural perturbations due to Y9P substitution (and importantly to the polyprotein construction itself; Figure 2D) would be limited to the mechanical intermediate, leaving the main mechanical clamp identical to that of I27wt as no new NOEs between L8 NH and ^{1}H atoms of residues from the mechanical clamp were observed in I27Y9P, in agreement with its reported monomeric structure (Yagawa et al., 2010). Thus, our structural data do not reveal new or alternative H bonds or other structural features in the I27Y9P variant that could justify the high mechanical stability previously reported (Li et al., 2000b).

The Global Stability of I27Y9P Is Lower

The relative instabilities of the I27Y9P monomer and polyprotein were determined by thermal denaturation monitored by circular dichroism (Figure S4) and NMR-monitored H/D exchange (Figure S3). I27wt proved to be more thermostable than I27Y9P (in line with published bulk results; Yagawa et al., 2010) and both polyproteins are less stable than their corresponding monomers. Whereas monomer thermal denaturation seemed reversible, polyprotein unfolding was irreversible; this is probably related to the formation of misfolded species (Borgia et al., 2011). Due to this irreversibility, we were not able to obtain reliable thermodynamic parameters (Table 1). Nevertheless, the apparent T_m values, although dependent on pH and ionic strength (Politou et al., 1995), indicate that polyproteins are less heat stable than the corresponding monomers. Interestingly, our data agree with the reported reorganization of the hydrophobic core due to the Y9P substitution, which results in a more exposed core and therefore a lower global stability (Yagawa et al., 2010).

$(I27Y9P)_{12}$ Has Similar Mechanical Stability than $(I27wt)_{12}$ but No Mechanical Intermediate

We next wanted to test the mechanical effect on the unfolding intermediate suggested by our polyprotein structural data. To this end, we first analyzed by SMFS the mechanical properties of $(I27wt)_{12}$ (Carrión-Vázquez et al., 1999) and $(I27Y9P)_{12}$ polyproteins in the same experimental conditions previously used to describe I27Y9P nanomechanics, namely PBS (pH 7.4) and a pulling speed of 0.6–0.8 nm/ms (Li et al., 2000b; Figure 3), to confirm the reported higher mechanical stability of I27Y9P. In these conditions, $(I27wt)_{12}$ showed the expected mechanical properties, i.e., an unfolding intermediate (observed as a deviation from the worm-like chain [WLC] fitting to the main force peak; Figure 3A; Bustamante et al., 1994; Marko and Siggia, 1995) with values of increase in contour length (ΔL_c) and unfolding force (F_u) that were comparable with those previously reported (Figures 3A, 3C, and 3D; Table 1; Marszalek et al., 1999) and a main unfolding peak corresponding to the rupture of the A′-G patch (Lu et al., 1998; Carrión-Vázquez et al.,

Table 1. Summary of Stability Data

Protein	F_u NaP 0.8 nm/ms (pN)	F_u PBS 0.8 nm/ms (pN)	F_u PBS 0.4 nm/ms (pN)	F SMD 1 Å/ps (pN)	ΔG (cal/M)	m (cal/M mol)	T_m (°C)	$\Delta\Delta G$ (cal/mol)
I27wt	ND	ND	202 ± 33 (in pFS + I27wt)	345 ± 69 (1TIT) 376 ± 37 (1WAA)	940 ± 180	−200 ± 40	71.3 ± 0.1	–
$(I27wt)_{12}$	120 ± 28 (N→I) 210 ± 36 (I→U)	128 ± 22 (N→I) 214 ± 23 (I→U)	118 ± 18 (N→I) 195 ± 24 (I→U)	ND	1,270 ± 430	−210 ± 70	63.1 ± 0.1	ND
I27Y9P	ND	ND	206 ± 41 (in pFS + I27Y9P)	362 ± 51 (2RQ8)	580 ± 550	−180 ± 100	64.3 ± 0.1	−1970 ± 60
$(I27Y9P)_{12}$	212 ± 32 (N→U)	220 ± 30 (N→U)	202 ± 36 (N→U)	ND	1,250 ± 990	−310 ± 260	59.8 ± 0.1	ND

NaP stands for sodium phosphate buffer (see Supplemental Experimental Procedures). At 0.4 nm/ms, the $(I27wt)_{12}$ intermediate showed a ΔL_c of 1.8 ± 0.5 nm (n = 49), and its main unfolding peak a ΔL_c value of 27.3 ± 0.5 nm (n = 83). Meanwhile, at this pulling speed, $(I27Y9P)_{12}$ showed a ΔL_c value of 27.3 ± 0.2 nm (n = 149). The T_m value for I27wt is the reference value for calculating the stability changes of the other constructs, $\Delta\Delta G$ ($\Delta\Delta G \approx \Delta S \cdot \Delta T_m$). Note that T_m has been described to strongly depend on pH and ionic strength, at least for I27wt (Politou et al., 1995).See also Figures S4, S5 and S7.

1999), with the expected ΔL_c and F_u values. Much to our surprise, $(I27Y9P)_{12}$ showed F_u values that were significantly lower than those previously reported (Li et al., 2000b). Indeed, this variant showed an F_u value similar to that of I27wt, within the experimental uncertainty (Figures 3B and 3D; Table 1). Moreover, similar to other Ig titin modules (Li and Fernández, 2003), this protein did not show any deviation from the WLC fitting (Figures 3B and 3C), which indicates that there are no detectable intermediate states in $(I27Y9P)_{12}$ mechanical unfolding, as our polyprotein NMR data suggested. Similar properties were observed when these polyproteins were stretched at a lower pulling speed (0.4 nm/ms; Table 1), in spite of the lower F_u values obtained in these conditions (which is expected, as F_u depends on the pulling speed; Carrión-Vázquez et al., 2006).

The discrepancy of our results with those previously reported in the value of mechanical stability (Li et al., 2000b) could have arisen from different factors; for instance, systematic errors originated from the calibration of a single cantilever used to obtain most of the dataset. This would explain the much wider force distribution obtained in that study for this mutant in comparison with that of the other proline mutants or the wild-type.

To rule out the possibility that electrostatic interactions between $(I27Y9P)_{12}$ repeats affect the SMFS unfolding results (Figure 2H; Politou et al., 1994, 1996; Scott et al., 2002; Rounsevell et al., 2005), we repeated the SMFS experiments at a higher ionic strength, using the same buffer conditions as for the thermal denaturation experiments (100 mM sodium phosphate buffer/150 mM NaCl [pH 7.5]; see Experimental Procedures). The mechanical properties of $(I27Y9P)_{12}$ were absolutely comparable in these new conditions (Figures 3E and 3F; Table 1), which suggests that the alleged electrostatic interactions between adjacent modules of the polyprotein, if present, do not affect its mechanical stability.

To further test if the presence of adjacent modules may affect the mechanical properties of I27Y9P subunits in the polyprotein, we cloned the monomers in a novel expression vector that was designed by our group for a more accurate SMFS analysis (pFS-1; Figure 4A and 4B; Oroz et al., 2012). As this vector is composed of ubiquitin repeats (as single-molecule marker) in series with an unstructured protein whose mechanical stability is lower than that of I27, these elements will unfold prior to I27. Thus, any possible interaction initially present between modules in the pFS will be disrupted before the I27 module unfolds. Furthermore, the insertion site for I27wt and I27Y9P was identical, which means that any linker effect (residues TS and AR remained at each side) would be comparable in both cases. The mechanical properties (ΔL_c and F_u values) of I27wt and I27Y9P measured in these constructs were, once again, absolutely comparable (Figure 4 and Table 1). We note that no I27wt or I27Y9P intermediates were detected in these experiments due to the intermediate's small contribution to ΔL_c (only 6.6 Å per module, Marszalek et al., 1999). Thus, all the evidence supports the conclusion that I27Y9P is comparable with I27wt in main mechanical stability. Since these results do not agree with previously published work, we approached two different laboratories to repeat the experiments using different AFMs, which corroborated our results (Figure S5; Acknowledgments).

Simulations Provide the Details on the Mechanical Unfolding Pathway of I27Y9P

Finally, to obtain putative atomic details of the unfolding of I27wt and I27Y9P, we performed steered molecular dynamics (SMD) simulations using the generalized Born surface area (GBSA) approximation (Figure 5), as previously described (Valbuena et al., 2009). We ran 10 ns of free molecular dynamics and performed six stretching simulations for I27Y9P (PDB: 2RQ8; Yagawa et al., 2010; Figure S6A) and I27wt (using both PDB: 1TIT and 1WAA as starting atomic structures; Improta et al., 1996; Stacklies et al., 2009; Figures S6B and S6C). The average force values observed for all the structures under our simulation conditions were similar (Table 1). In the case of I27wt, we were able to reproduce the main unfolding events as previously reported (Figures 5B and 5C; Lu et al., 1998; Lu and Schulten, 2000). However, in the case of I27Y9P, the first force peak (the unfolding intermediate), if present, showed a markedly reduced amplitude that is almost indistinguishable from the noise of the trace (Figure 5B), and at this point the A-B backbone H-bonded patch still had not ruptured (Figure 5D). The high force peak recorded corresponded to the simultaneous rupture of A-B and A′-G backbone H-bonded patches. These calculations serve to illustrate the similar mechanical properties of I27wt and I27Y9P monomers and polyproteins observed experimentally (Figures 3 and 4). Thus, our simulations of I27Y9P closely and qualitatively reproduce the experimental results; although the intermediate's structural hallmarks are present in the monomer, its population is very low to negligible during stretching and the forces of the main

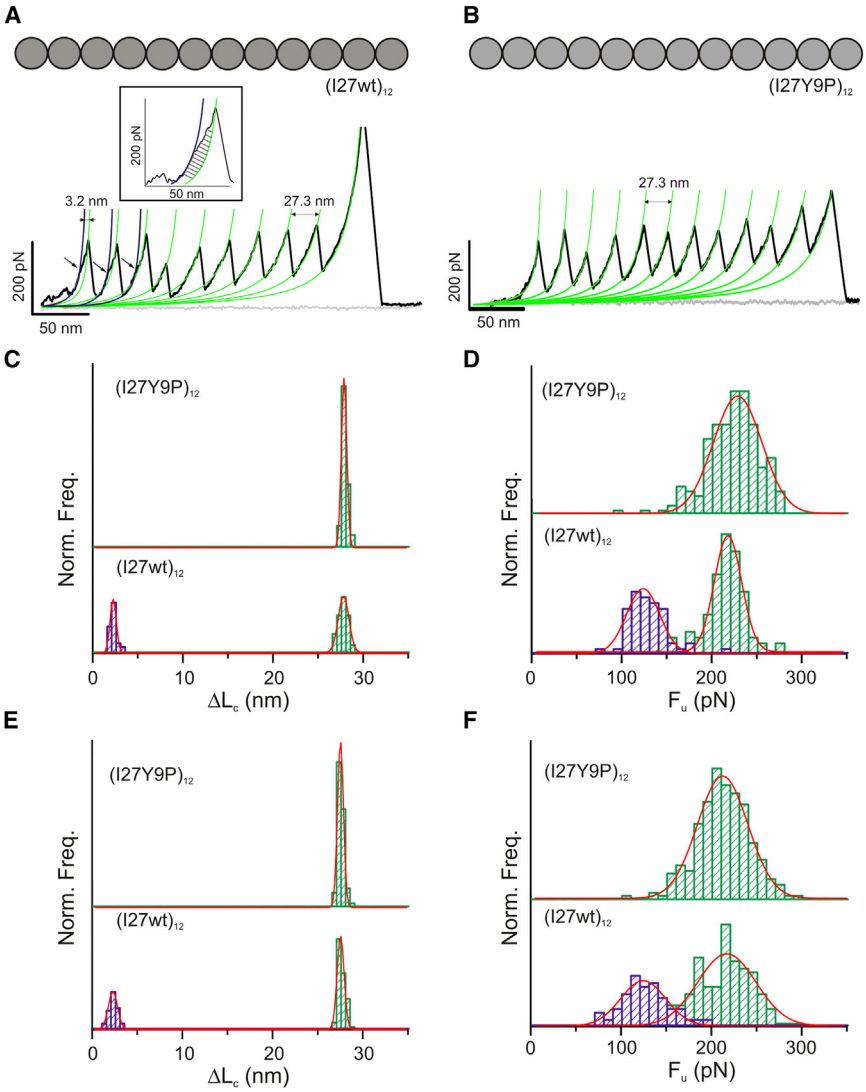

Figure 3. SMFS Analysis of Homomeric Polyproteins: $(I27wt)_{12}$ and $(I27Y9P)_{12}$

(A) $(I27wt)_{12}$ typical force-extension curve. The green lines correspond to the fit of the WLC model (with a ΔL_c of 27.3 nm) to the main unfolding event, while the dark blue lines correspond to the fit of the unfolding of the intermediate state, observed as a deviation from the single family of WLC curve fitting (see inset). Note the decreasing amplitude of this intermediate with successive module unfolding (Marszalek et al., 1999).

(B) A typical $(I27Y9P)_{12}$ force-extension curve. No intermediate state is observed here.

(C and D) ΔL_c (C) and F_u (D) histograms for $(I27wt)_{12}$ (bottom) and $(I27Y9P)_{12}$ (top) in PBS (pH 7.4) and a pulling speed of 0.8 nm/ms. $(I27wt)_{12}$ mechanical intermediate state (blue histograms) showed a ΔL_c value of 2.0 ± 0.4 nm (n = 54), while the main unfolding peak (green histograms) showed a ΔL_c of 27.5 ± 0.8 nm (n = 89). $(I27Y9P)_{12}$ showed a ΔL_c of 27.7 ± 0.3 nm (n = 172), and comparable F_u values with $(I27wt)_{12}$ (Table 1).

(E and F) ΔL_c (E) and F_u (F) histograms for $(I27wt)_{12}$ and $(I27Y9P)_{12}$ in 100 mM sodium phosphate, 150 mM NaCl buffer (pH 7.5), and 0.8 nm/ms of pulling speed. The mechanical intermediate of $(I27wt)_{12}$ showed a ΔL_c of 2.0 ± 0.5 nm (n = 81), while the main unfolding peak showed a ΔL_c of 27.3 ± 0.4 nm (n = 164). On the other hand, $(I27Y9P)_{12}$ showed a ΔL_c of 27.3 ± 0.4 nm (n = 326) and comparable F_u values (Table 1). Gaussian fits to histograms are shown in red.

See also Figures S5 and S7.

rupture event are comparable with those of I27wt. That patch could be missing in $(I27Y9P)_{12}$ according to the NMR data and indeed no mechanical intermediate is observed experimentally (Figures 2 and 3).

Our SMFS and SMD data suggest that, for I27Y9P, the mechanical intermediate state is not stable enough to constitute a discreet state, and thus its mechanical unfolding pathway can be modeled as a two-state process ($N_I \rightarrow U$) instead of the three-state process described for I27wt ($N \rightarrow I \rightarrow U$, Williams et al., 2003). This means that for I27Y9P, the step measured by SMFS is $N_I \rightarrow U$, rather than $I \rightarrow U$, as occurs for I27wt (Fowler et al., 2002; Williams et al., 2003). In order to further characterize the I27Y9P unfolding process, we studied the unfolding kinetic parameters of the polyprotein and compared them with those of I27wt. To that end, we studied the dependence of the F_u with the pulling speed and performed Monte Carlo simulations (Carrión-Vázquez et al., 1999). Interestingly, we found that the slope of this dependence was similar in wild-type and mutant and thus the mutant showed comparable kinetic parameters (Figure S7). Taken together, our data support an energy landscape model in which the wild-type I27 and I27Y9P mutant would share the main unfolding event, with comparable energy and Δx_U for both proteins. Thus, in the I27Y9P, since the native state is destabilized, the molecule is found in a state equivalent to the intermediate state of the wild-type and therefore only one barrier is observed, which corresponds to the rupture of the A′-G patch of H bonds (Figure 6).

It has been postulated that the Y9P substitution mechanically stabilizes the N terminus by improving the packing of hydrophobic side chains in this zone (Yagawa et al., 2010). This would explain the simultaneous rupture of the A-B and A′-G backbone H bond patches observed in the I27Y9P simulations (Figure 5D; Best et al., 2003; Sharma et al., 2008; Stacklies et al., 2009; Yagawa et al., 2010). However, our polyprotein data indicate structural rearrangements and a significant loss of stability in this region (Figures 2 and S3). In any case, even if the A-B patch is present, it cannot account for the previously reported higher mechanical stability for I27Y9P (Li et al., 2000b).

Apparently, a similar effect could explain the mechanical phenotype of I27K6P (Marszalek et al., 1999; Yagawa et al., 2010), which is similar to that of I27Y9P described here, and for other Ig titin modules (Li and Fernández, 2003). Interestingly, when these variants were used as substrates for mitochondrial translocases, they showed a reduced rate of processing compared with I27wt when the unfolding process started at

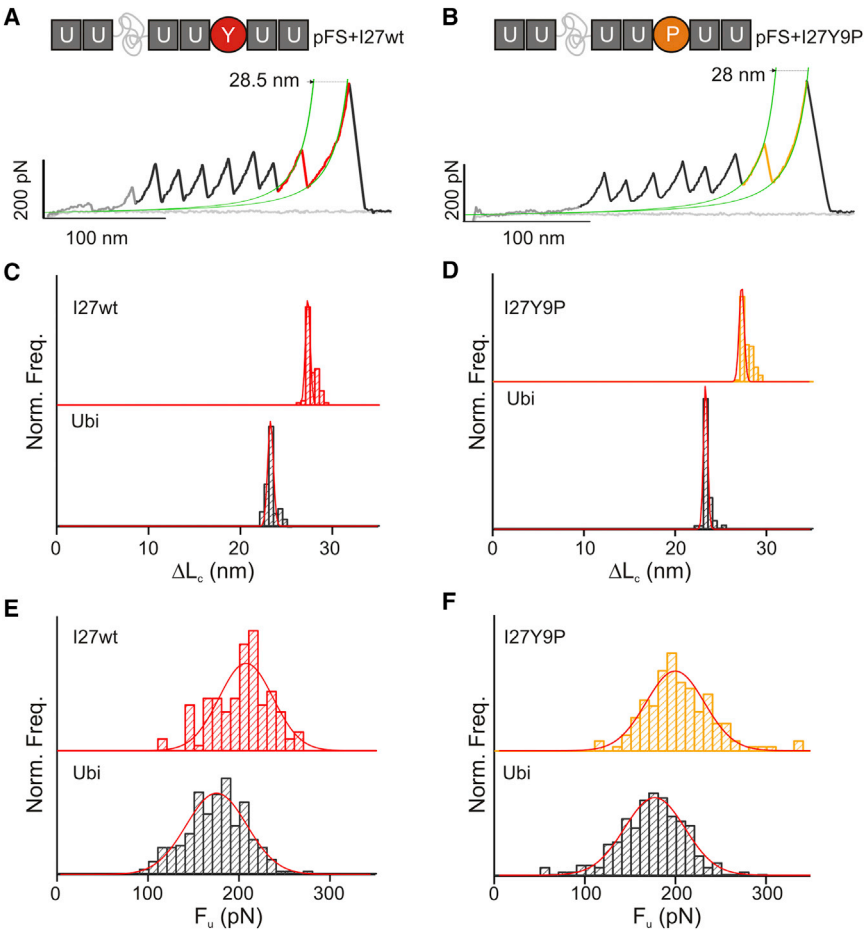

Figure 4. SMFS Analysis of Heteromeric Polyproteins: pFS + I27wt and pFS + I27Y9P

(A) Schematic representation of pFS + I27wt polyprotein. Ubiquitin repeats are represented as gray boxes with a U inside. The N2B polypeptide present in pFS-1 is represented as a light gray coiled coil (Oroz et al., 2012). This color code is maintained through the rest of this figure. The I27wt module is represented as a red circle, indicated with the Y for Y9. The force-extension recording shows that the N2B segment and the ubiquitin repeats (gray force peaks) unfold before the I27wt module (red force peak showing its fitting to the WLC, in green).

(B) Schematic representation of the pFS + I27Y9P polyprotein. I27Y9P module is represented as an orange circle, indicated with the P for P9.

(C) ΔL_c histograms of ubiquitin repeats (gray histogram, bottom, n = 345) and I27wt module (red histogram, top, n = 101) from pFS + I27wt. Ubiquitin repeats showed a ΔL_c of 23.0 ± 0.5 nm, while I27wt showed a ΔL_c of 27.4 ± 0.6 nm.

(D) ΔL_c histograms of pFS + I27Y9P. Ubiquitin repeats showed a ΔL_c of 23.2 ± 0.5 nm (n = 297) and I27Y9P showed a ΔL_c of 27.5 ± 0.6 nm (n = 118).

(E) F_u histograms of pFS + I27wt. Ubiquitin repeats showed a F_u of 174 ± 33 pN, while I27wt showed a F_u of 202 ± 33 pN.

(F) F_u histograms of pFS + I27Y9P polyprotein. Ubiquitin repeats showed a F_u of 173 ± 39 pN, and I27Y9P a F_u of 206 ± 41 pN, and thus forces were comparable with I27wt. All the data in this figure were collected in PBS (pH 7.4) at a pulling speed of 0.4 nm/ms. No intermediate was observed in these proteins due to its small size in monomeric I27wt (Marszalek et al., 1999). Gaussian fits to histograms are shown in red.

See also Figure S5.

the N terminus (due to the stabilization in this region), but similar rates when the process started at the C terminus (due to a similar mechanical stability; Sato et al., 2005; Oguro et al., 2009; Yagawa et al., 2010). Therefore, our data indicate a close correlation between mechanical stability, as measured by SMFS, and the resistance to processing from these unfolding machineries (the AAA^+-ATPase-based machineries are known to unfold their substrate proteins mechanically; Aubin-Tam et al., 2011; Maillard et al., 2011, Cordova et al., 2014), despite the differences in the pulling geometry between translocases and AFM (Wilcox et al., 2005). In any case, during its possible unfolding under physiological mechanical stress in the heart muscle, I27 would feel mechanical force applied to both of its termini, as occurs in SMFS, and not just at one end, as happens in the translocase assays.

Conclusions and Future Prospects

The standard strategy in SMFS to select bona fide single-molecule recordings relies on utilizing either homomeric polyproteins of the protein of interest, or heteromeric polyproteins with the protein of interest fused to protein repeats that act as single-molecule markers (Carrión-Vázquez et al., 1999, 2006; Li et al., 2001; Oroz et al., 2012). Several lines of evidence strongly suggest that the structure of an individual protein module is not affected when it is inserted inside a polyprotein, notwithstanding the possible formation of misfolded species (Oberhauser et al., 1999; Borgia et al., 2011). However, no experimental data, at atomic resolution, corroborating this assumption were available until now. Here, by high-resolution NMR, we show that titin I27wt, when arranged in a homomeric polyprotein, does not experience structural rearrangements or unspecific interactions between modules, whereas the I27Y9P variant definitely undergoes subtle structural rearrangements in these constructions. Furthermore, the structural data obtained can explain the observed thermal and mechanical stabilities. To our knowledge, this is the first time that a detailed structural analysis has been performed on long polyproteins, which has helped us to advance our understanding of the mechanical properties of I27Y9P. In addition, the example of I27Y9P, which shows a decreased thermal stability but similar mechanical stability relative to I27wt, corroborates the idea that the mechanical properties of a protein cannot be predicted by other denaturing techniques and must be directly measured by SMFS (Carrión-Vázquez et al., 2006).

The fact that no non-specific interactions are observable in I27wt polyproteins, in contrast to what occurs in other polyproteins (Rounsevell et al., 2005), may be related to the fact that this domain exists as a modular protein in nature and that, in

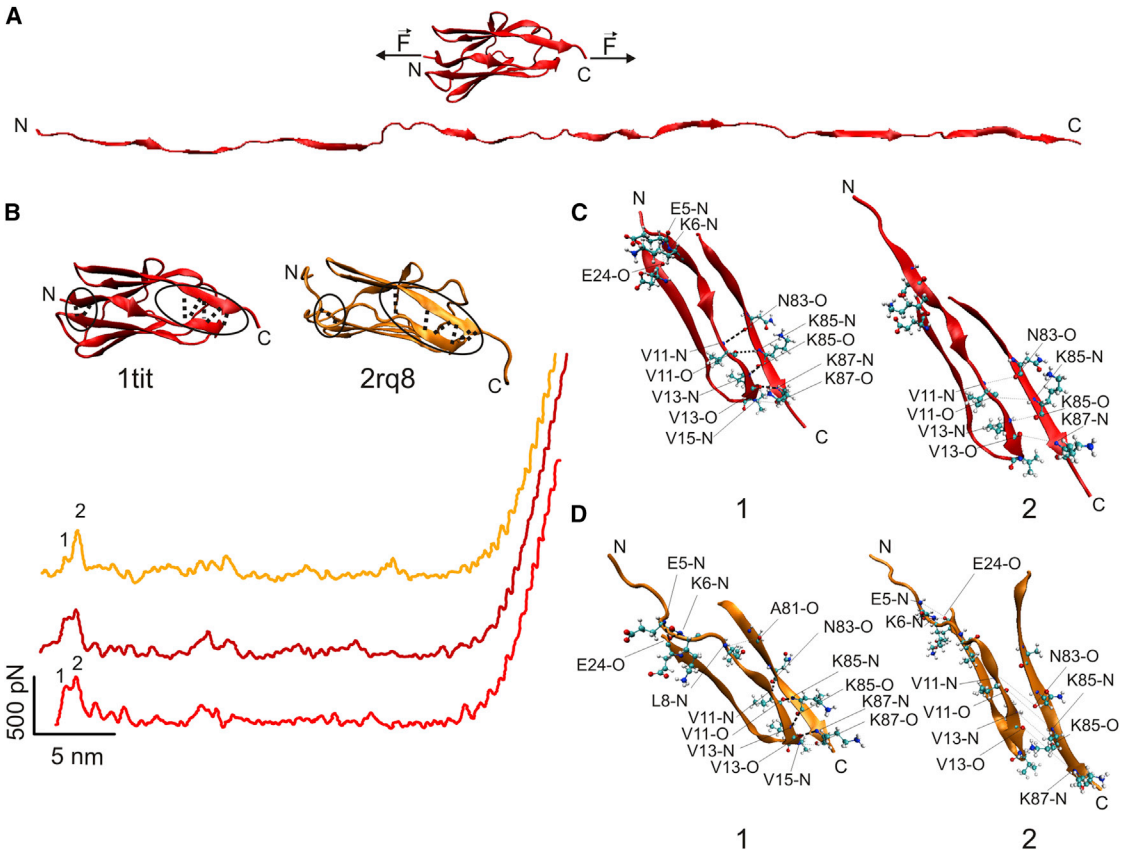

Figure 5. I27wt and I27Y9P Unfolding by SMD

(A) The I27wt structure (PDB: 1TIT; Improta et al., 1996) at the beginning (top) and the end (bottom) of its unfolding process as simulated by SMD.

(B) Top: representations of I27wt (left) and I27Y9P structures (right, PDB: 2RQ8; Yagawa et al., 2010), indicating the backbone H bonds (black dashes) that constitute the mechanical clamps of the modules found during most of the free molecular dynamics (see Supplemental Experimental Procedures). The H bond between Y9-N83 reported in I27wt (Lu and Schulten, 2000) was not found in our simulations. Bottom: representative force traces of I27wt (PDB: 1TIT, bottom, red; and PDB: 1WAA, middle, dark red; Stacklies et al., 2009) and I27Y9P structures (PDB: 2RQ8, top, orange) obtained from stretching simulations, showing a main force peak with comparable magnitude (Figure S6). Numbers represent the main mechanical resistance barriers found during unfolding, 1 for the mechanical intermediate and 2 for the main unfolding peak. The intermediate state in I27Y9P is indistinguishable from the noise of the trace.

(C) Backbone H bond rupture during the main force events found in I27wt (PDB: 1TIT) unfolding. In 1, only bonds between E5-, K6-E24 (A-B β strands), and V15-K87 were broken (in gray) producing the intermediate force peak, while the simultaneous rupture of V11-N83, V11-K85, V13-K85, and V13-K87 occurs in 2, leading to the main force peak. These results reproduce those previously reported (Lu and Schulten, 2000).

(D) Details of backbone H bond rupture during the main force events found in I27Y9P (PDB: 2RQ8) unfolding. Only L8-A81 (observed in this particular stretching) and V15-K87 bonds were broken in 1, the A-B patch is maintained. In 2, all the H bonds remaining between A-B and A′-G β strands are simultaneously broken, leading to the force peak. A possible N-terminal stabilization in I27Y9P (Yagawa et al., 2010) could lead to this simultaneous rupture, and thus the loss of a visible intermediate. In (C) and (D), N stands for backbone amide HN, while O stands for carbonyl oxygen.

See also Figure S6.

physiological conditions, it could unfold individually (Linke and Grützner, 2008). The ability to resolve this structural individuality of I27 inside a polyprotein by NMR allows us to extend this kind of analysis to other modular proteins with mechanical function. Accordingly, we could obtain a more native-like structure that includes the real boundaries of the module under study (Varadan et al., 2002; von Castelmur et al., 2008). Moreover, this approach could become a very useful structural control of the polyprotein strategy in SMFS, which is important since usually the determinants of mechanical stability in mechanical proteins are located near the protein's termini and could be affected by linking them into a polyprotein (Politou et al., 1994; Scott et al., 2002; Rounsevell et al., 2005). More interestingly, our results on polyprotein NMR suggest that NMR could be very useful in the future to get high-resolution structural information from large (>120 kDa) pseudo-polyproteins with high identity among their modules.

Finally, the multidisciplinary approach reported here (which combines SMFS with high-resolution structural techniques as well as thermal stability measurements and simulations) should allow us to get further insight into the relationship between mechanical stability and structural perturbations, which could result, for instance, from extramodular elements (Oroz et al., 2011), ligand binding (Ainavarapu et al., 2005), mutations (Ma et al., 2009), or an intrinsic conformational polymorphism (Hervás et al., 2012). Indeed, the growing understanding of the link between mechanical stability and protein structure is already being used in protein engineering for the successful design of

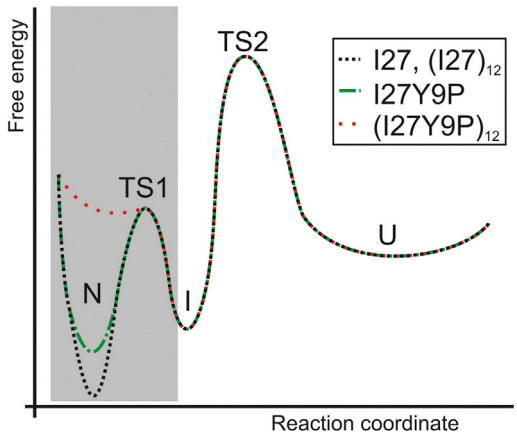

Figure 6. Proposed Energy Diagram for the Mechanical Unfolding of I27Y9P

The I27wt module (black) shows three states (native, N; intermediate, I; unfolded, U) where the A-B patch of H bonds is broken in the intermediate state (I). In the case of the I27Y9P mutant (monomer, green), the ground state (N) is destabilized and hence the energy barrier of the I state is reduced, and in the polyprotein (red), the energy barrier has disappeared or is residual since the native state (N) is destabilized (it is not observed experimentally). Therefore, the main determinant for mechanical stability for both proteins ($N_I \rightarrow U$ for I27Y9P and $I \rightarrow U$ for I27wt, corresponding to the rupture of the A′-G patch) is similar. In this representation, we assume changes only in the ground state, although there could also be changes in the transition state (TS1) that could change the height of the energy barrier. This more speculative region of the diagram is indicated with a shaded box.
See also Figure 3 and Figure S7.

proteins with the desired mechanical properties (Sharma et al., 2007; Ng et al., 2007; Borgia et al., 2008).

EXPERIMENTAL PROCEDURES

Cloning, Expression, ^{15}N-Labeling and Purification of the Recombinant Proteins

To test whether the atomic structure of I27 (wt and Y9P) was preserved in the polyproteins used for SMFS, we had to use polyproteins with identical linkers between repeats to facilitate the comparison with the corresponding monomer (Figures 1, 2, and S1). To this end, for NMR analyses, we used a plasmid sequence containing eight repeats of I27wt in a pQE30 vector (Qiagen), which contains identical sequences between repeats (coding for RS; Carrión-Vázquez et al., 1999), and a home-made plasmid containing 12 I27Y9P repeats (pET-AvaI, with the LG sequence between repeats; Li et al., 2000b). This $(I27Y9P)_{12}$ clone was also used for SMFS and thermal stability measurements (Figures 3 and S4). The latter home-made plasmid was also used to prepare an I27wt construct containing 12 repeats for thermal stability and SMFS analyses (Carrión-Vázquez et al., 1999). Regarding the monomers, we cloned the I27wt coding sequence (Carrión-Vázquez et al., 1999) inside pET28a plasmid (Novagen). To clone I27Y9P, a similar PCR cloning approach was employed except that a 5′ primer containing the Y9P substitution was used. To build pFS + I27wt and pFS + I27Y9P sequences (Figure 4), the aforementioned I27wt and I27Y9P monomeric sequences were cloned between SpeI-BssHII sites in pFS-1 vector (Oroz et al., 2012). Details of protein production, purification, and characterization are described in Supplemental Experimental Procedures.

NMR Spectroscopy

The δ (Figure 2) and NOE data were obtained from 2D ^{1}H-^{15}N-HSQC, 3D ^{1}H-^{15}N NOESY and 3D ^{1}H-^{15}N total correlation spectroscopy (TOCSY) for the monomeric (I27wt and I27Y9P) and polyprotein ($(I27wt)_8$ and $(I27Y9P)_{12}$) samples. The ^{15}N-labeled samples were dissolved in 100 mM NaCl, 2 mM β-mercaptoethanol with 10% D_2O (pH 4.5), to the following final concentrations: 0.7 mM (I27wt), 1 mM (I27Y9P), 0.1 mM ($(I27wt)_8$), and 0.2 mM ($(I27Y9P)_{12}$). Experiments were performed at 25°C in a Bruker AV 800 spectrometer (Bruker BioSpin), equipped with a *z*-gradient cryoprobe. 2,2-dimethyl-2-silapentane-5-sulfonate ($(CH_3)_3$-Si-CH_2-CH_2-CH_2-$SO_3^-Na^+$) (DSS) was used as the internal δ reference (Markley et al., 1998). Δδ values were calculated according to the equation, $[\Delta\delta(^{1}H)^2 + (\Delta\delta(^{15}N)/5)^2]^{1/2}$, and those residues showing values larger than 1 SD are highlighted (Figure 2). Spectra were acquired and Fourier transformed with the Topspin 2.1 program (Bruker BioSpin) and analyzed using Sparky 3.114 (Goddard, T.D., and Kneller, D.G.. SPARKY 3. University of California).

SMFS

For SMFS experiments, a drop of the protein preparation (~10–20 μl of a solution at 0.2–0.5 mg/ml) was applied on top of a drop of the corresponding experimental buffer (PBS, 137 mM NaCl/2.7 mM KCl/10 mM $Na_2HPO_4 \cdot 2H_2O$/2 mM KH_2PO_4 [pH 7.4] or 100 mM sodium phosphate buffer/150 mM NaCl [pH 7.5]; Figures 3 and 4) placed onto the substrate, which was either gold-coated (commercial Arrandee gold-coated substrates, Gold Arrandee) or nitrilotriacetic acid-Ni^{2+} functionalized coverslips (Hervás et al., 2012), and allowed to adsorb for 10–20 min. Both substrates rendered identical results. Our custom-made AFM, with added imaging capabilities, and its mode of operation are described elsewhere (Valbuena et al., 2009). Details of the experimental conditions, data acquisition, and analysis are described in Supplemental Experimental Procedures.

SMD Simulations

The GBSA approach uses implicit solvent to simulate water molecules as a continuum, with surface access corrections (Tsui and Case, 2001). A detailed method of this approach starting from PDB structures in order to perform free molecular dynamics was reported elsewhere (Valbuena et al., 2009). Further details of the SMD simulations are described in Supplemental Experimental Procedures.

SUPPLEMENTAL INFORMATION

Supplemental Information includes Supplemental Experimental Procedures, seven figures, and one table and can be found with this article online at http://dx.doi.org/10.1016/j.str.2016.02.016.

ACKNOWLEDGMENTS

We thank Armando Albert (Instituto de Química-Física Rocasolano, CSIC) and Jesús Mendieta (Centro de Biología Molecular Severo-Ochoa, CSIC) for helpful discussions in the initial phase of this project. The repetition of SMFS experiments in different AFMs by Víctor Muñoz (Centro Nacional de Biotecnología, CSIC and University of California, Merced) and Andrés Oberhauser (University of Texas Medical Branch) is also acknowledged. The authors also thank the members of M.C.-V.'s laboratory for critical reading of the manuscript. This work was funded by grants from the Ministerio de Economía y Competitividad (MINECO-SAF2013-49179-C2-1-R and ERA-NET grant ERA-IB EIB.12.022, FiberFuel), the EC (FP7-NMP604530-2, CellulosomePlus), to M.C.-V., and grants from the MINECO to M.B. (CTQ2014-52633-P), D.V.L. (MINECO-SAF2013-49179-C2-2-R) and F.J.C. (CTQ2009-08536, CTQ2012-32025). J.O. was a recipient of a fellowship from the Consejería de Educación de la Comunidad de Madrid and is currently recipient of a Marie Curie IEF fellowship, while A.G.P. was a recipient of an FPU fellowship from the MINECO.

Received: June 25, 2013
Revised: November 30, 2015
Accepted: February 22, 2016
Published: March 24, 2016

REFERENCES

Ainavarapu, S.R.K., Li, L., Badilla, C.L., and Fernández, J.M. (2005). Ligand binding modulates the mechanical stability of dihydrofolate reductase. Biophys. J. *89*, 3337–3344.

Aubin-Tam, M.E., Olivares, A.O., Sauer, R.T., Baker, T.A., and Lang, M.J. (2011). Single-molecule protein unfolding and translocation by an ATP-fueled proteolytic machine. Cell *145*, 257–267.

Bang, M.L., Centner, T., Fornoff, F., Geach, A.J., Gotthardt, M., McNabb, M., Witt, C.C., Labeit, D., Gregorio, C.C., Granzier, H., and Labeit, S. (2001). The complete gene sequence of titin, expression of an unusual approximately 700-kDa titin isoform, and its interaction with obscurin identify a novel Z-line to I-band linking system. Circ. Res. *89*, 1065–1072.

Batey, S., and Clarke, J. (2008). The folding pathway of a single domain in a multidomain protein is not affected by its neighbouring domain. J. Mol. Biol. *378*, 297–301.

Best, R.B., Li, H.B., Steward, A., Daggett, V., and Clarke, J. (2001). Can non-mechanical proteins withstand force? Stretching barnase by atomic force microscopy and molecular dynamics simulation. Biophys. J. *81*, 2344–2356.

Best, R.B., Fowler, S.B., Toca-Herrera, J.L., Steward, A., Paci, E., and Clarke, J. (2003). Mechanical unfolding of a titin Ig domain: structure of transition state revealed by combining atomic force microscopy, protein engineering and molecular dynamics simulations. J. Mol. Biol. *330*, 867–877.

Borgia, A., Steward, A., and Clarke, J. (2008). An effective strategy for the design of proteins with enhanced mechanical stability. Angew. Chem. Int. Ed. Engl. *47*, 6900–6903.

Borgia, M.B., Borgia, A., Best, R.B., Steward, A., Nettels, D., Wunderlich, B., Schuler, B., and Clarke, J. (2011). Single-molecule fluorescence reveals sequence-specific misfolding in multidomain proteins. Nature *474*, 662–665.

Brockwell, D.J., Beddard, G.S., Clarkson, J., Zinober, R.C., Blake, A.W., Trinick, J., Olmsted, P.D., Smith, D.A., and Radford, S.E. (2002). The effect of core destabilization on the mechanical resistance of I27. Biophys. J. *83*, 458–472.

Bustamante, C., Marko, J.F., Siggia, E.D., and Smith, S. (1994). Entropic elasticity of lambda-phage DNA. Science *265*, 1599–1600.

Carrión-Vázquez, M., Oberhauser, A.F., Fowler, S.B., Marszalek, P.E., Broedel, S.E., Clarke, J., and Fernández, J.M. (1999). Mechanical and chemical unfolding of a single protein: a comparison. Proc. Natl. Acad. Sci. USA *96*, 3694–3699.

Carrión-Vázquez, M., Oberhauser, A.F., Fisher, T.E., Marszalek, P.E., Li, H., and Fernández, J.M. (2000). Mechanical design of proteins studied by single-molecule force spectroscopy and protein engineering. Prog. Biophys. Mol. Biol. *74*, 63–91.

Carrión-Vázquez, M., Oberhauser, A.F., Díez, H., Hervás, R., Oroz, J., Fernández, J., and Martínez-Martín, D. (2006). Protein nanomechanics – as studied by AFM single-molecule force spectroscopy. In Advanced Techniques in Biophysics, J.L.R. Arrondo and A. Alonso, eds. (Springer-Verlag), pp. 163–245.

Cecconi, C., Shank, E.A., Bustamante, C., and Marqusee, S. (2005). Direct observation of the three-state folding of a single protein molecule. Science *309*, 2057–2060.

Cordova, J.C., Olivares, A.O., Shin, Y., Stinson, B.M., Calmat, S., Schmitz, K.R., Aubin-Tam, M.-E., Baker, T.A., Lang, M.J., and Sauer, R.T. (2014). Stochastic but highly coordinated protein unfolding and translocation by the ClpXP proteolytic machine. Cell *158*, 647–658.

Feng, G., and Lu, H. (2007). Computer simulation of I27 translocation through ClpY reveals a critical role of protein mechanical strength and local stability. Conf. Proc. IEEE Eng. Med. Biol. Soc. *2007*, 1213–1216.

Fowler, S.B., and Clarke, J. (2001). Mapping the folding pathway of an immunoglobulin domain: structural detail from phi value analysis and movement of the transition state. Structure *9*, 355–366.

Fowler, S.B., Best, R.B., Toca-Herrera, J.L., Rutherford, T.J., Steward, A., Paci, E., Karplus, M., and Clarke, J. (2002). Mechanical unfolding of a titin Ig domain: structure of unfolding intermediate revealed by combining AFM, molecular dynamics simulations, NMR and protein engineering. J. Mol. Biol. *322*, 841–849.

García-Manyes, S., Brujic, J., Badilla, C.L., and Fernández, J.M. (2007). Force-clamp spectroscopy of single-protein monomers reveals the individual unfolding and folding pathways of I27 and ubiquitin. Biophys. J. *93*, 2436–2446.

Gautel, M., Lehtonen, E., and Pietruschka, F. (1996). Assembly of the cardiac I-band region of titin/connectin: expression of the cardiac specific regions and their structural relation to the elastic segments. J. Muscle Res. Cell. Motil. *17*, 449–461.

Hervás, R., Oroz, J., Galera-Prat, A., Goñi, O., Valbuena, A., Vera, A.M., Gómez-Sicilia, A., Losada-Urzáiz, F., Uversky, V.N., Menéndez, M., et al. (2012). Common features at the start of the neurodegeneration cascade. PLoS Biol. *10*, e1001335.

Improta, S., Politou, A.S., and Pastore, A. (1996). Immunoglobulin-like modules from titin I-band: extensible components of muscle elasticity. Structure *4*, 323–337.

Kenniston, J.A., Baker, T.A., Fernández, J.M., and Sauer, R.T. (2003). Linkage between ATP consumption and mechanical unfolding during the protein processing reactions of an AAA+ degradation machine. Cell *114*, 511–520.

Kenniston, J.A., Baker, T.A., and Sauer, R.T. (2004). Partitioning between unfolding and release of native domains during ClpXP degradation determines substrate selectivity and partial processing. Proc. Natl. Acad. Sci. USA *102*, 1390–1395.

Labeit, S., and Kolmerer, B. (1995). Titins: giant proteins in charge of muscle ultrastructure and elasticity. Science *270*, 293–296.

Li, H., and Fernández, J.M. (2003). Mechanical design of the first proximal Ig domain of human cardiac titin revealed by single molecule force spectroscopy. J. Mol. Biol. *334*, 75–86.

Li, H., Oberhauser, A.F., Fowler, S.B., Clarke, J., and Fernández, J.M. (2000a). Atomic force microscopy reveals the mechanical design of a modular protein. Proc. Natl. Acad. Sci. USA *97*, 6527–6531.

Li, H., Carrión-Vázquez, M., Oberhauser, A.F., Marszalek, P.E., and Fernández, J.M. (2000b). Point mutations alter the mechanical stability of immunoglobulin modules. Nat. Struct. Biol. *7*, 1117–1120.

Li, H., Oberhauser, A.F., Redick, S., Carrión-Vázquez, M., Erickson, H.P., and Fernández, J.M. (2001). Multiple conformations of PEVK proteins detected by single-molecule techniques. Proc. Natl. Acad. Sci. USA *98*, 10682–10686.

Linke, W.A., and Grützner, A. (2008). Pulling single molecules of titin by AFM – recent advances and physiological implications. Eur. J. Physiol. *456*, 101–115.

Linke, W.A., Ivemeyer, M., Olivieri, N., Kolmerer, B., Rüegg, J.C., and Labeit, S. (1996). Towards a molecular understanding of the elasticity of titin. J. Mol. Biol. *261*, 62–71.

Lu, H., and Schulten, K. (2000). The key event in force-induced unfolding of titin's immunoglobulin domains. Biophys. J. *79*, 51–65.

Lu, H., Isralewitz, B., Krammer, A., Vogel, V., and Schulten, K. (1998). Unfolding of titin immunoglobulin domains by steered molecular dynamics simulation. Biophys. J. *75*, 662–671.

Ma, L., Xu, M., Forman, J.R., Clarke, J., and Oberhauser, A.F. (2009). Naturally occurring mutations alter the stability of polycystin-1 PKD domains. J. Biol. Chem. *284*, 32942–32949.

Maillard, R.A., Chistol, G., Sen, M., Righini, M., Tan, J., Kaiser, C.M., Hodges, C., Martin, A., and Bustamante, C. (2011). ClpX(P) generates mechanical force to unfold and translocate its protein substrates. Cell *145*, 459–469.

Markley, J.L., Bax, A., Arata, Y., Hilbers, C.W., Kaptein, R., Sykes, B.D., Wright, P.E., and Wüthrich, K. (1998). Recommendations for the presentation of NMR structures of proteins and nucleic acids. J. Biomol. NMR *12*, 1–23.

Marko, J.F., and Siggia, E.D. (1995). Stretching DNA. Macromolecules *28*, 8759–8770.

Marszalek, P.E., Lu, H., Li, H., Carrión-Vázquez, M., Oberhauser, A.F., Schulten, K., and Fernández, J.M. (1999). Mechanical unfolding intermediates in titin modules. Nature *402*, 100–103.

Ng, S.P., Billings, K.S., Ohashi, T., Allen, M.D., Best, R.B., Randles, L.G., Erickson, H.P., and Clarke, J. (2007). Designing an extracellular matrix protein with enhanced mechanical stability. Proc. Natl. Acad. Sci. USA *104*, 9633–9637.

Oberhauser, A.F., Marszalek, P.E., Carrión-Vázquez, M., and Fernández, J.M. (1999). Single protein misfolding events captured by atomic force microscopy. Nat. Struct. Biol. *6*, 1025–1028.

Oguro, T., Yagawa, K., Momose, T., Sato, T., Yamano, K., and Endo, T. (2009). Structural stabilities of different regions of the titin I27 domain contribute differently to unfolding upon mitochondrial protein import. J. Mol. Biol. *385*, 811–819.

Oroz, J., Valbuena, A., Vera, A.M., Mendieta, J., Gómez-Puertas, P., and Carrión-Vázquez, M. (2011). Nanomechanics of the cadherin ectodomain: "canalization" by Ca^{2+} binding results in a new mechanical element. J. Biol. Chem. *286*, 9405–9418.

Oroz, J., Hervás, R., and Carrión-Vázquez, M. (2012). Unequivocal single-molecule force spectroscopy of proteins by AFM using pFS vectors. Biophys. J. *102*, 682–690.

Paci, E., and Karplus, M. (2000). Unfolding proteins by external forces and temperature: the importance of topology and energetics. Proc. Natl. Acad. Sci. USA *97*, 6521–6526.

Politou, A.S., Gautel, M., Joseph, C., and Pastore, A. (1994). Immunoglobulin-type domains of titin are stabilized by amino-terminal extension. FEBS Lett. *352*, 27–31.

Politou, A.S., Thomas, D.J., and Pastore, A. (1995). The folding and stability of titin immunoglobulin-like modules with implications for the mechanism of elasticity. Biophys. J. *69*, 2601–2610.

Politou, A.S., Gautel, M., Improta, S., Vangelista, L., and Pastore, A. (1996). The elastic I-band of titin is assembled in a "modular" fashion by weakly interacting Ig-like domains. J. Mol. Biol. *255*, 604–616.

Randles, L.G., Batey, S., Steward, A., and Clarke, J. (2008). Distinguishing specific and nonspecific interdomain interactions in multidomain proteins. Biophys. J. *94*, 622–628.

Rief, M., Gautel, M., Oesterhelt, F., Fernández, J.M., and Gaub, H.E. (1997). Reversible unfolding of individual titin immunoglobulin domains by AFM. Science *276*, 1109–1112.

Rounsevell, R.W.S., Steward, A., and Clarke, J. (2005). Biophysical investigations of engineered polyproteins: implications for force data. Biophys. J. *88*, 2022–2029.

Ruprecht, M., Bionda, T., Sato, T., Sommer, M.S., Endo, T., and Schleiff, E. (2010). On the impact of precursor unfolding during protein import into chloroplasts. Mol. Plant *3*, 499–508.

Sato, T., Esaki, M., Fernández, J.M., and Endo, T. (2005). Comparison of the protein-unfolding pathways between mitochondrial protein import and atomic force microscopy measurements. Proc. Natl. Acad. Sci. USA *102*, 17999–18004.

Scott, K.A., Steward, A., Fowler, S.B., and Clarke, J. (2002). Titin; a multidomain protein that behaves as the sum of its parts. J. Mol. Biol. *315*, 819–829.

Sharma, D., Perisic, O., Peng, Q., Cao, Y., Lam, C., Lu, H., and Li, H. (2007). Single-molecule force spectroscopy reveals a mechanically stable protein fold and the rational tuning of its mechanical stability. Proc. Natl. Acad. Sci. USA *104*, 9278–9283.

Sharma, D., Feng, G., Khor, D., Genchev, G.Z., Lu, H., and Li, H. (2008). Stabilization provided by neighboring strands is critical for the mechanical stability of proteins. Biophys. J. *95*, 3935–3942.

Shin, Y., Davis, J.H., Brau, R.R., Martin, A., Kenniston, J.A., Baker, T.A., Sauer, R.T., and Lang, M.J. (2009). Single-molecule denaturation and degradation of proteins by the AAA+ ClpXP protease. Proc. Natl. Acad. Sci. USA *106*, 19340–19345.

Stacklies, W., Vega, M.C., Wilmanns, M., and Gräter, F. (2009). Mechanical network in titin immunoglobulin from force distribution analysis. PLoS Comp. Biol. *5*, e1000306.

Tripp, K.W., and Barrick, D. (2004). The tolerance of a modular protein to duplication and deletion of internal repeats. J. Mol. Biol. *344*, 169–178.

Tsui, V., and Case, D.A. (2001). Theory and applications of the generalized Born solvation model in macromolecular simulations. Biopolymers *56*, 275–291.

Valbuena, A., Oroz, J., Hervás, R., Vera, A.M., Rodríguez, D., Menéndez, M., Sulkowska, J.I., Cieplak, M., and Carrión-Vázquez, M. (2009). On the remarkable mechanostability of scaffoldins and the mechanical clamp motif. Proc. Natl. Acad. Sci. USA *106*, 13791–13796.

Varadan, R., Walker, O., Pickart, C., and Fushman, D. (2002). Structural properties of polyubiquitin chains in solution. J. Mol. Biol. *324*, 637–647.

von Castelmur, E., Marino, M., Labeit, D., Labeit, S., and Mayans, O. (2008). A regular pattern of Ig super-motifs defines segmental flexibility as the elastic mechanism of the titin chain. Proc. Natl. Acad. Sci. USA *105*, 1186–1191.

Wilcox, A.J., Choy, J., Bustamante, C., and Matouschek, A. (2005). Effect of protein structure on mitochondrial import. Proc. Natl. Acad. Sci. USA *102*, 15435–15440.

Williams, P.M., Fowler, S.B., Best, R.B., Toca-Herrera, J.L., Scott, K.A., Steward, A., and Clarke, J. (2003). Hidden complexity in the mechanical properties of titin. Nature *422*, 446–449.

Wright, C.F., Lindorff-Larsen, K., Randles, L.G., and Clarke, J. (2003). Parallel protein-unfolding pathways revealed and mapped. Nat. Struct. Biol. *10*, 658–662.

Yagawa, K., Yamano, K., Oguro, T., Maeda, M., Sato, T., Momose, T., Kawano, S., and Endo, T. (2010). Structural basis for unfolding pathway-dependent stability of proteins: Vectorial unfolding versus global unfolding. Protein Sci. *19*, 693–702.

Structure, Volume *24*

Supplemental Information

The Y9P Variant of the Titin I27 Module: Structural Determinants of Its Revisited Nanomechanics

Javier Oroz, Marta Bruix, Douglas V. Laurents, Albert Galera-Prat, Jörg Schönfelder, Francisco Javier Cañada, and Mariano Carrión-Vázquez

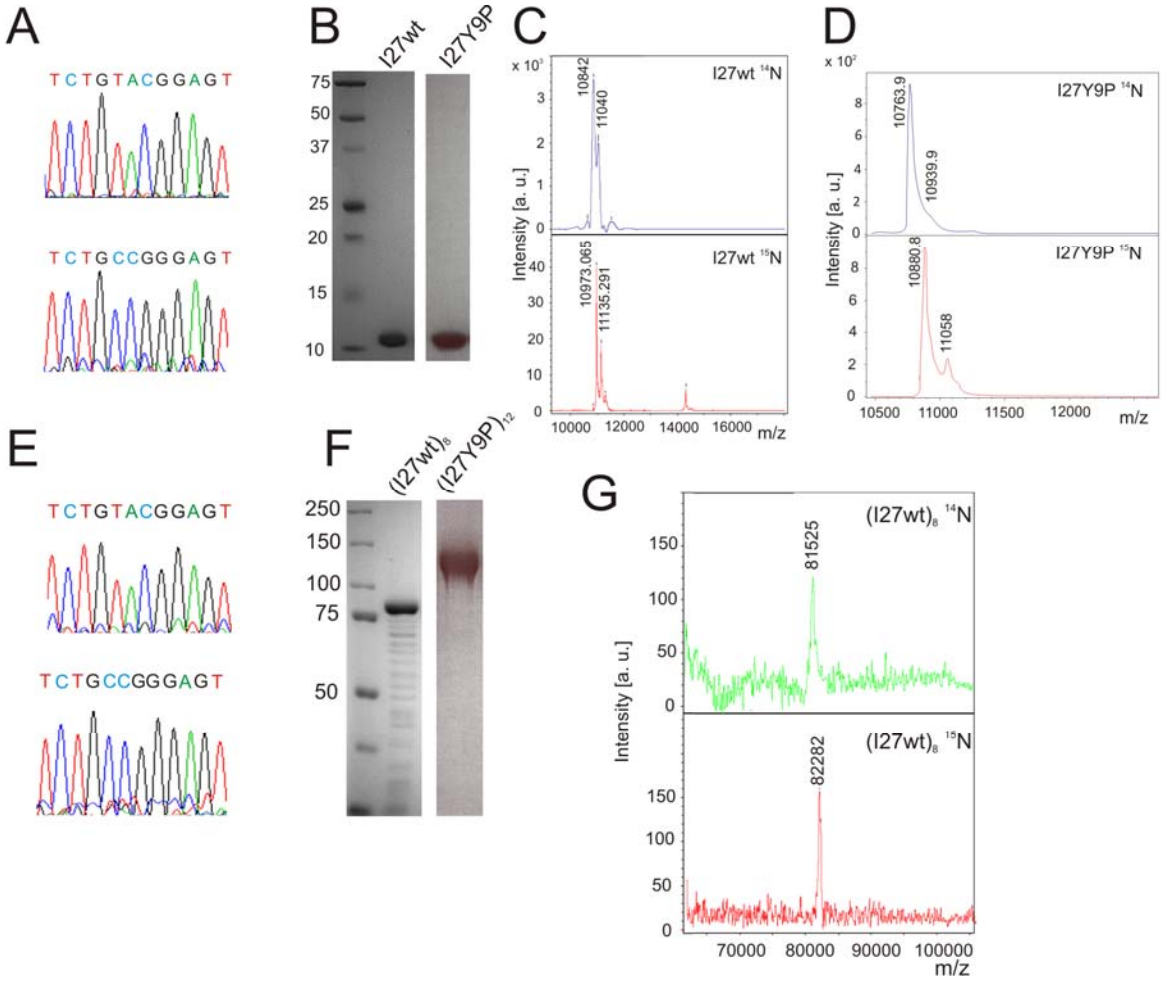

Figure S1. Related to Figures 1, 2, S2, S3 and S4. ^{15}N-labelling for NMR spectroscopy. A) Sequencing chromatograms for I27wt (top) and I27 Y9P (bottom) monomers. The sequence detail shown here verifies the Y9P substitution (TAC→CCG). **B)** ^{15}N-labelled I27wt and I27 Y9P monomers observed in Coomassie Blue-stained 15% SDS-PAGE. According to ProtParam (http://www.expasy.org/tools/protparam.html), both proteins have a nominal size of 11 kDa. **C-D)** MALDI-TOF spectra for ^{14}N and ^{15}N-labelled I27wt (**C**) and I27Y9P monomers (**D**). The ^{15}N incorporation was 97% and 87% in I27wt and I27Y9P, respectively. Both molecules contain a total of 135 nitrogen atoms, and the mass corresponding to full isotopic enrichment was calculated by an increase of 0.996 Da per nitrogen atom in the protein. Whereas the extra peak observed in the I27wt spectra is of unknown origin, the extra peak observed in the I27Y9P spectra (with an increase of ~177 Da) could be due to the typical α-N-6-Phosphogluconoylation of His-tagged proteins that occurs in *E. coli* (Geoghegan et al., 1999). **E)** Sequencing chromatograms for $(I27wt)_8$ (top) and $(I27Y9P)_{12}$ (bottom), showing the TAC→CCG substitution. Both sequences were taken from random repeats in the polyprotein. **F)** Purified ^{15}N $(I27wt)_8$ and $(I27Y9P)_{12}$ observed in Coomassie-Blue stained 8% SDS-PAGE. According to ProtParam, nominal sizes are 82 kDa for $(I27wt)_8$ and 121 kDa for $(I27Y9P)_{12}$. **G)** MALDI-TOF spectra for ^{14}N and ^{15}N-labelled $(I27wt)_8$ revealing 78% ^{15}N incorporation in the latter. $(I27wt)_8$ contains 973 nitrogen atoms. It was not possible to quantify ^{15}N incorporation in $(I27Y9P)_{12}$ in MALDI-TOF due to its large size (> 100 kDa).

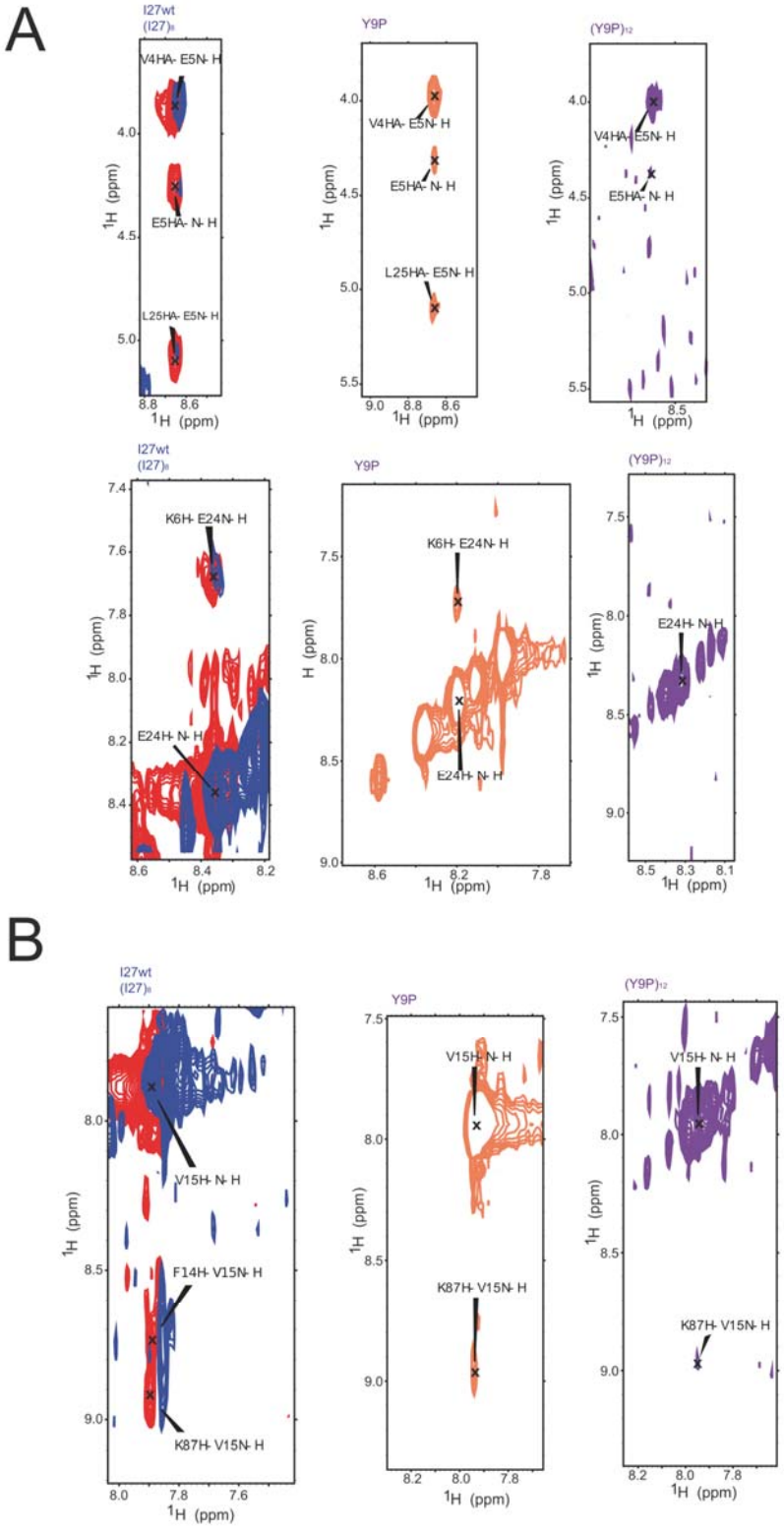

Figure S2. Related to Figure 2. Representative NOEs from residues located in the A-B (mechanical intermediate, A) and A'-G (mechanical clamp, B) patches. Whereas the same NOEs were found in I27wt (red), $(I27wt)_8$ (blue) and I27Y9P (orange), the lack of NOEs between the residues contained in the A-B patch in $(I27Y9P)_{12}$ (**A**, right, in purple) indicate a structural rearrangement in this region leading to the modification of this patch. The NOEs observed between residues contained in the A'-G patch (**B**) are maintained in $(I27Y9P)_{12}$ indicating that this region is not affected. Thus this data perfectly correlate with the lack of mechanical intermediate but identical F_u observed for $(I27Y9P)_{12}$. The spectra corresponding to $(I27wt)_8$ (blue) is intentionally upfield shifted in ^{1}H dimension for clarity.

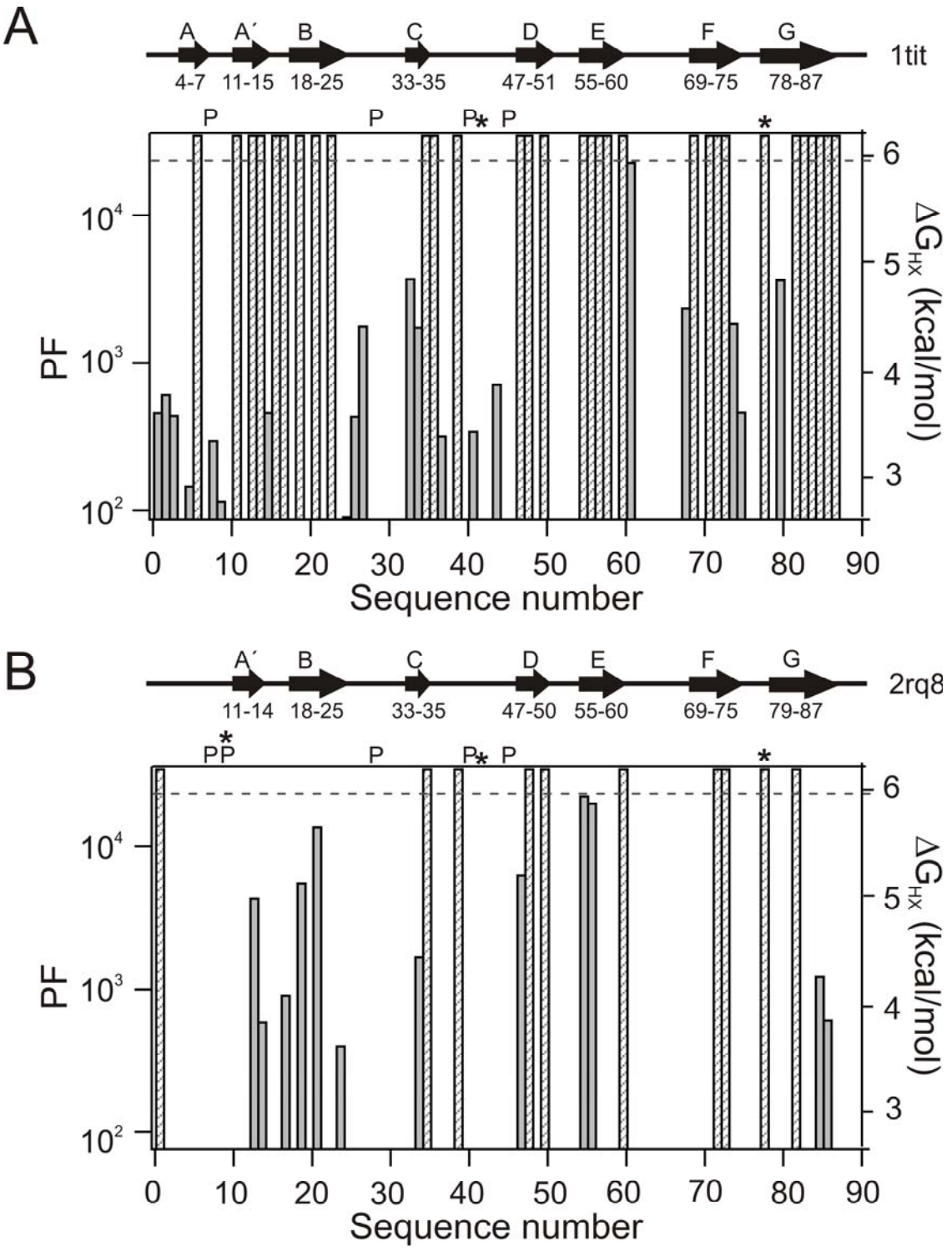

Figure S3. Related to Figure 2. Polyprotein conformational free energy measured by H/D exchange. In both panels, strongly protected HNs that exchange incompletely with solvent deuterons are shown in grey hashed bars, and no bars are shown for HN groups whose exchange is complete in the experimental dead time. **A)** $(I27wt)_8$ amide proton PF values (left axis) and conformational free energy (right). The grey horizontal dotted line shows the highest PF value measured in our experiments, corresponding to H61 ($PF = 2.3 \cdot 10^4$; $\Delta G_{HX} = 5.95$ kcal/mol). The most protected residues ($\Delta G_{HX} > 6$ kcal/mol) correlate with I27wt β-strands, represented as arrows at the top of the panel. P means proline, and the asterisks indicate the substitutions compared to 1tit. **B)** $(I27Y9P)_{12}$ conformational free energy. The exchange of many HNs is faster in $(I27Y9P)_{12}$ than in $(I27wt)_8$, indicating that $(I27Y9P)_{12}$ is less conformationally stable. As explained in **Supplemental Information**, due to a longer dead time before the first spectra was acquired for $(I27Y9P)_{12}$ only H-N crosspeaks signals corresponding to more protected HNs could be monitored.

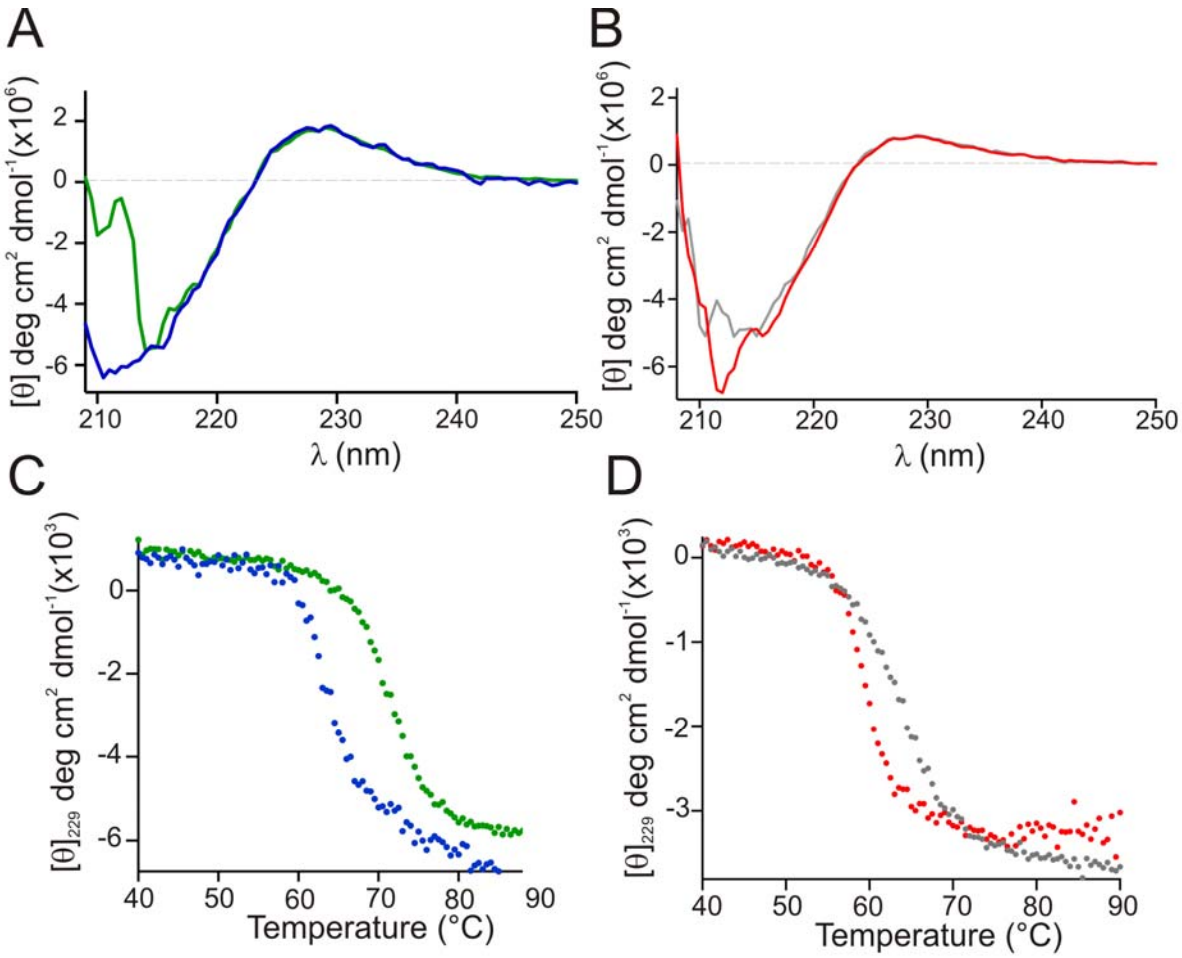

Figure S4. Related to Table 1. Thermal denaturation analysis. A) Monomeric I27wt (green) and $(I27wt)_{12}$ (blue) CD spectra at 25 ºC. **B)** Monomeric I27 Y9P (grey) and $(I27\ Y9P)_{12}$ (red) CD spectra at 25 ºC, showing (as in **A**) a typical all-β CD spectra. The color code here and in (**A**) is maintained through the rest of the figure. **C)** Thermal denaturation curves for I27wt and $(I27wt)_{12}$, as monitored by [θ] changes at 229 nm. $(I27wt)_{12}$ is less thermally stable than I27wt (**Table 1**). **D)** Thermal denaturing curve for I27Y9P and $(I27Y9P)_{12}$, as monitored by [θ] changes at 229 nm. Once again, the polyprotein is less thermally stable than the monomer.

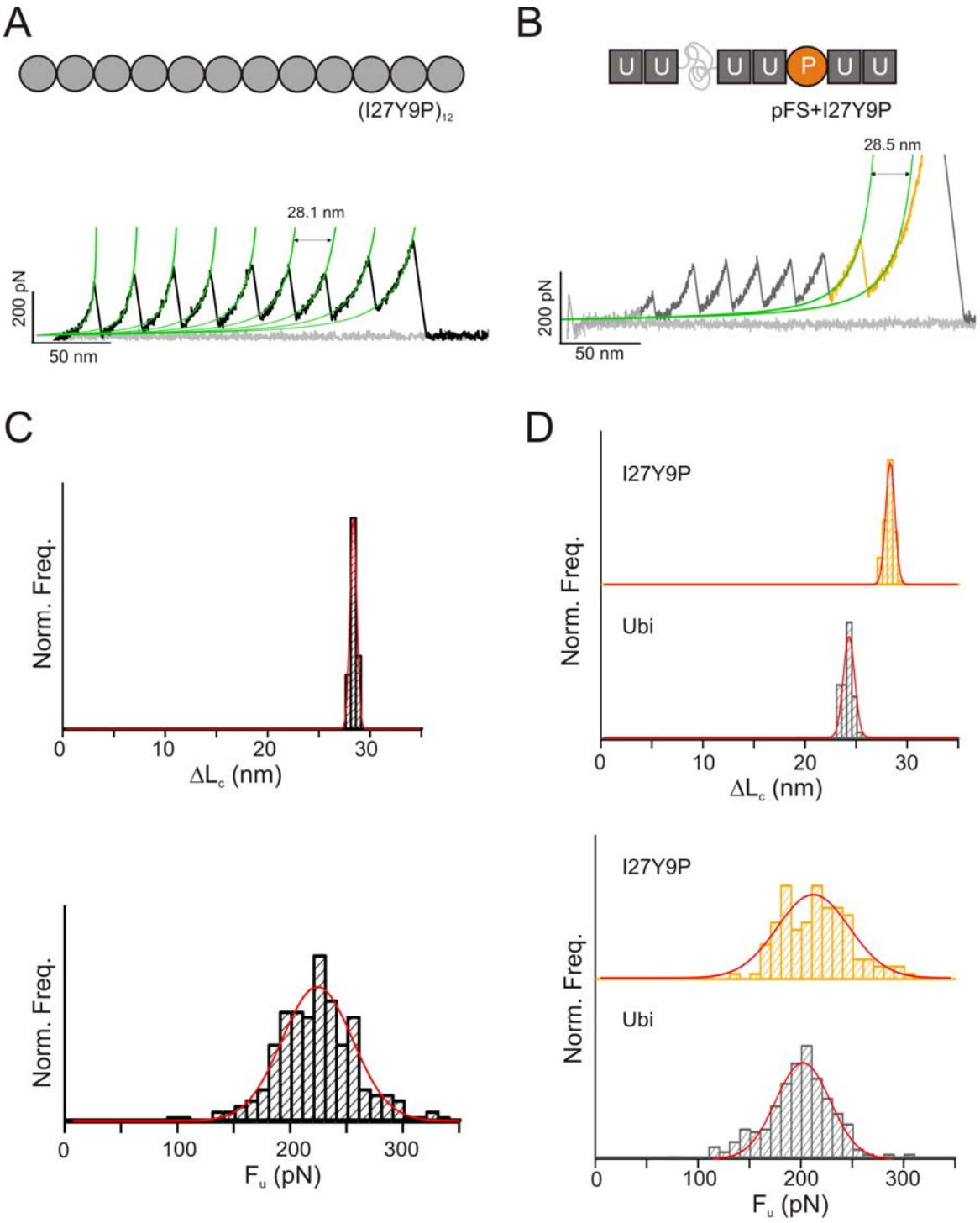

Figure S5. Related to Figures 3 and 4 and Table 1. Repetition of SMFS experiments. Since our SMFS data turned out surprising based on the values reported previously (**Figures 4, 5**; Li et al., 2000b), we repeated our experiments with I27Y9P in two different laboratories and AFMs to confirm the values reported in the main text (see **Supplemental Experimental Procedures**). Both results were comparable; here we show the ones obtained in the laboratory of Prof. Víctor Muñoz. $(I27\ Y9P)_{12}$ (**A**) and pFS+ I27Y9P (**B**) proteins were pulled in the same conditions as described in the main text. The $(I27\ Y9P)_{12}$ polyprotein (**C**) showed a ΔL_c value of 28.3 ± 0.3 nm and 222 ± 37 pN of F_u (n= 201), similar values to those reported in **Table 1** and **Figure 4**. Moreover, I27 Y9P monomer showed a ΔL_c value of 27.9 ± 0.5 nm and 216 ± 34 pN of F_u (n= 98) in the pFS+Y9P construction (**D**), similar to values reported in **Table 1**. Interestingly, the ubiquitin repeats present in pFS showed here a slightly higher F_u value (198 ± 34 pN; with 23.8 ± 0.5 nm of ΔL_c, n= 283), which could be related with the force being slightly overestimated in these measurements due to the higher noise of this apparatus. The color code in this figure corresponds to that followed in **Figures 4, 5**.

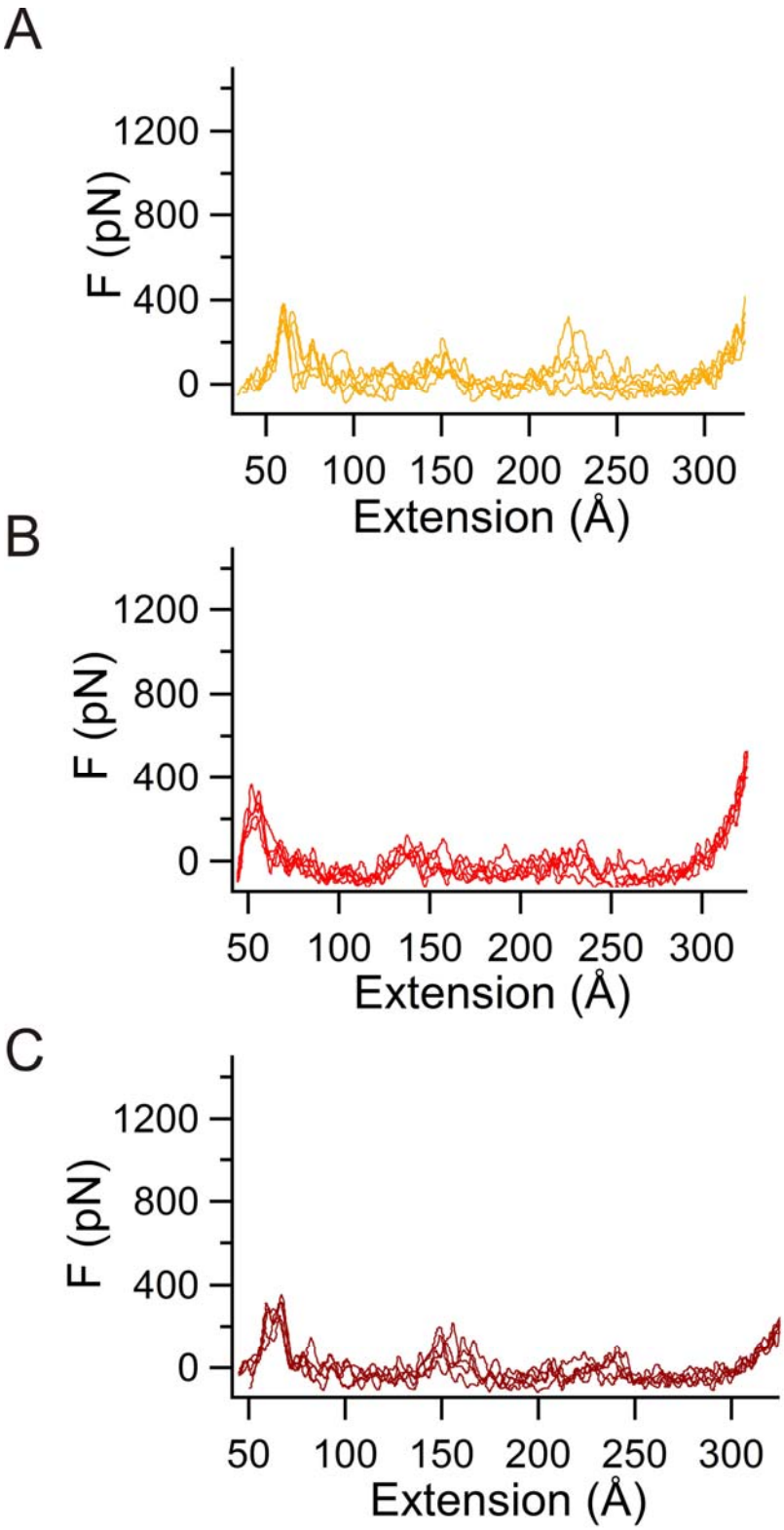

Figure S6. Related to Figure 5. Overlay of the force-extension curves obtained by SMD. All the force-extension curves obtained by SMD were plotted for I27 Y9P (PDB code 2rq8, top; Yagawa et al., 2010; **A**) and I27wt (PDB code 1tit, red; Improta et al., 1996; **B**; and PDB code 1waa, dark red; Stacklies et al., 2009; **C**). All of them show comparable force values (**Table 1**), and in the curves for I27wt, both force peaks (intermediate and main unfolding peak) can be observed (particularly in **C**, probably due to the presence of novel stabilizing interactions in N-terminus owing to the T78A mutation in 1waa, which is not present in 1tit; Stacklies et al., 2009).

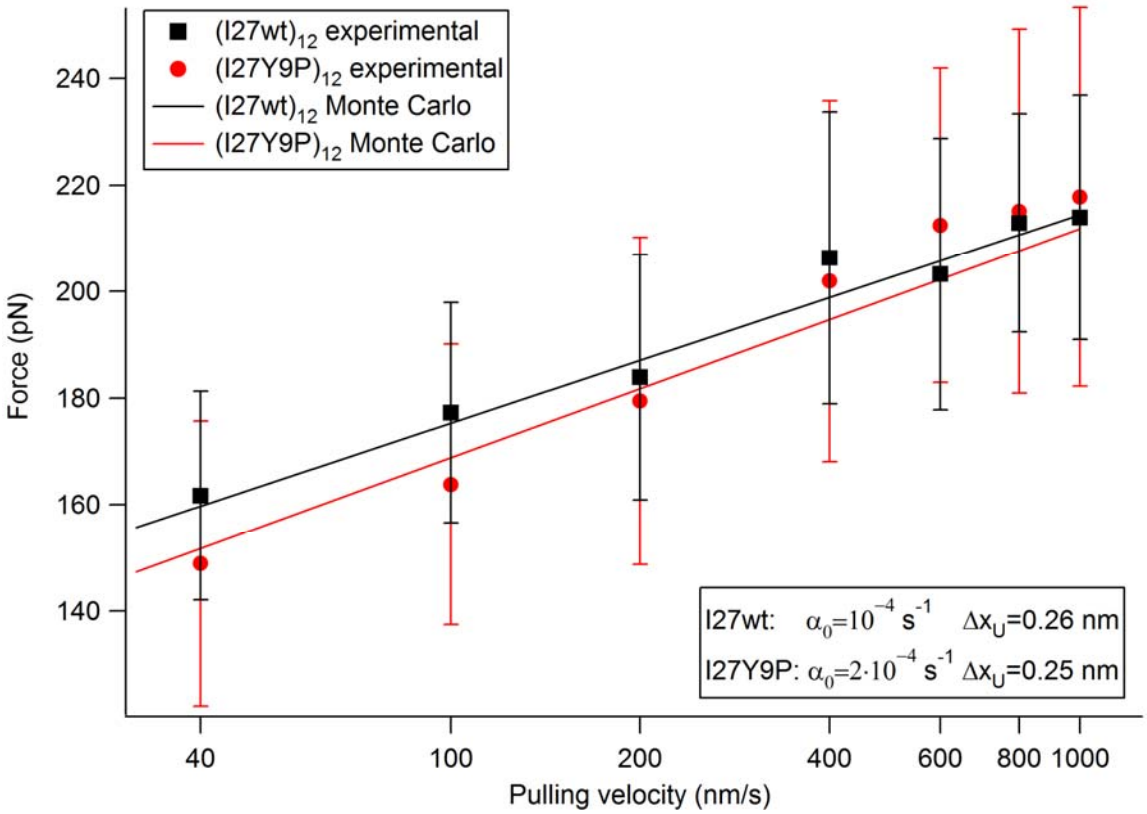

Figure S7. Related to Figures 3 and 6. Unfolding force dependence on the pulling speed for I27Y9P. The unfolding force at different pulling speeds was measured for $(I27wt)_{12}$ (black squares) and $(I27Y9P)_{12}$ (red squares). The unfolding force distributions of $(I27wt)_{12}$ and $(I27Y9P)_{12}$ were very similar at the studied pulling speeds. The kinetic parameters were estimated by performing Monte Carlo simulations of the mechanical unfolding process as previously described (Rief *et al.* 1998). The following values of α_0 and Δx_U closely reproduced the unfolding force distributions observed at the range of pulling speeds covered: I27 wt: $\alpha_0 = 10^{-4}s^{-1}$ and Δx_U 0.26 nm, I27Y9P: $\alpha_0 = 2{\cdot}10^{-4}s^{-1}$ and Δx_U 0.25 nm.

Reference	**Method**	**Sequence**	**Conditions**	**PDB file number**
Improta et al. (1996)	NMR	T42, A78	pH 4.5, 35 ºC 20 mM sodium acetate	1tit
Stacklies et al. (2009)	X-ray	A42, T78	pH 6.5, -173 ºC 20% PEG, 75 mM MES, 7.5 mM ZnSO4	1waa
Yagawa et al. (2010)	NMR	A42, T78 + Y9P	pH 7.4, 25 ºC 50 mM KPi	2rq8
This work	NMR	A42, T78 Y9 or P9	pH 4.5, 25 ºC 100 mM NaCl + 2 mM βME HX: pH 5.05 6.5 mM sodium acetate + 1 DTT	

Table S1. Related to Figure 1. Comparison of reported I27 structural studies and conditions.

Supplemental Experimental Procedures

Cloning, expression, ^{15}N-labelling and purification of the recombinant proteins

The two sequence substitutions contained in our I27wt (T42A, A78T) with respect to the 1tit sequence originally reported (Labeit and Kolmerer, 1995; deposited in ENA database; http://www.ebi.ac.uk/ena/, code CAA62188), were also present in the I27 sequence used in the pioneering SMFS experiments on titin (Rief et al., 1997). This sequence was later kept to build the I27 polyproteins (Carrión-Vázquez et al., 1999). It is unknown if these two changes represent a *bona fide* natural I27 isoform (not deposited in any database) or were the result of cloning artifacts in the original SMFS study. Indeed, the other two atomic structures described here (PDB codes 1waa and 2rq8) they both contain these changes, one of which (A78T) has been described to establish novel stabilizing interactions at the N-terminus of this module (Stacklies et al., 2009). We finally decided to maintain the described substitutions in the I27wt sequence in order to utilize identical sequences as those used in the literature to facilitate a closer comparison of the nanomechanical results. The pFS-1 vector used here is a slight modification of the sequence reported in the literature (it contains an additional N-terminal ubiquitin repeat). All the sequences (except the homomeric polyproteins) were verified by sequencing both strands of the DNA, and the cloning steps were carried out in the *E. coli* XL1-Blue strain (Stratagene). As $(I27Y9P)_{12}$ nanomechanical results were surprising to us, we decided to sequence part of this polyprotein. At least 9 out of the 12 I27Y9P repeats contained in the plasmid were sequenced and all of them were found to carry the correct mutated sequence (**Figure S1**).

The $(I27wt)_{12}$ and $(I27Y9P)_{12}$ proteins used for SMFS and thermal stability measurements were expressed in the BLR(DE3) *E. coli* strain (Novagen), while the monomer proteins used for thermal stability analyses were expressed in the BL21(DE3) strain (Novagen). Proteins based on pFS-1 were expressed in the C41(DE3) *E. coli* strain (Miroux and Walker, 1996). In all these cases, protein expression was induced for 3-4 hours by the addition of 1 mM IPTG to bacterial cultures after they reached an OD_{595} of 0.5-0.7. ^{15}N labelling for NMR of monomers and polyproteins was achieved following a previously described protocol (Marley et al., 2001) to optimize culture growth and for the incorporation of ^{15}N as $^{15}NH_4Cl$ (Cambridge Isotopes). The strain used in these cases was BL21(DE3), which showed the highest protein over-expression after IPTG induction. The incorporation of ^{15}N (97% for I27wt, 87% for I27 Y9P, ~78% for $(I27wt)_8$ was determined using MALDI-TOF-TOF Mass Spectrometry (**Figure S1**).

Bacterial pellets were lysed by treatment with 1 mg/ml lysozyme and 1% Triton X-100 (Sambrook et al., 1989). Recombinant proteins were purified by Ni^{2+}-affinity chromatography with Histrap HP (GE Healthcare) FPLC columns, using 50 mM sodium phosphate/500 mM NaCl [pH 7.4] buffer, added with 50 mM imidazole in the binding buffer and 500 mM imidazole in the elution buffer. Eluted fractions were concentrated by ultrafiltration using Amicon filters (Millipore), and they were subsequently purified by size exclusion chromatography using a Hiload 16/60 FPLC column (GE Healthcare). The buffer used in this purification step was 100 mM sodium phosphate/150 mM NaCl/1 mM DTT [pH 7.5]. Finally, purified samples were concentrated by ultrafiltration using Amicon filters and the buffer was exchanged to the appropriate one for the specific application. Protein purity was calculated to be >90% as determined by SDS-PAGE (**Figure S1**). Protein concentration was estimated by spectrophotometry using the corresponding molar extinction coefficient.

Hydrogen/Deuterium exchange by NMR spectroscopy

To further corroborate the conformation and stability of the polyproteins, we performed NMR-monitored H/D exchange experiments on $(I27wt)_8$ and $(I27Y9P)_{12}$ (**Supplemental Experimental Procedures**). These experiments should, in principle, allow us to assess whether the HN groups forming the putative backbone H-bonds show an increased resistance to exchange consistent with their bonding while HNs not participating in structural H-bonds exchange faster (Hermans et al., 1984; Huyghues-Despointes et al., 2001; Krishna et al., 2004). The corresponding protection factors (PF) and conformational free energies are shown in **Figure S3**. In the case of $(I27wt)_8$, the calculated PF values clearly show that the most protected residues are located in the secondary structures (β-strands; **Figure S3A**). $(I27Y9P)_{12}$ showed a general lower conformational thermal stability (**Figure S3B**) and the most protected regions show an arrangement comparable to the wt form. Consequently no evidences of newly formed H-bonds in $(I27Y9P)_{12}$ become apparent from H/D exchange experiments.

The exchange of amide protons with solvent deuterons was initiated by dissolving a lyophilized sample of protonated ^{15}N-(I27wt)$_8$ into deuterated solvent (6.5 mM sodium acetate/1 mM DTT). ^{15}N-(I27 Y9P)$_{12}$ showed high degradation following the aforementioned procedure. Therefore, this sample, dissolved in protonated buffer, was applied to a PD-10 gravity column (GE Healthcare) pre-equilibrated with deuterated buffer. Following elution, which exchanged the solvent protons for deuterons, the protein was concentrated using a Vivaspin filter (3 kDa cutoff, GE Healthcare). This longer processing time led to an increased exchange dead time (~130 min) and allowed more protein ^{1}H to exchange prior to the acquisition of the first NMR spectrum. These ^{1}H signals could be detected in ^{15}N-(I27wt)$_8$ due to the shorter dead time (~30 min) of the lyophilization procedure. The experimental temperature was 25 ºC, while the pH was set to 5.05 to favor exchange via the EX2 mechanism (Bruix et al., 2008). Hydrogen exchange rates were determined by integrating the volume of ^{1}H-^{15}N amide crosspeaks in a series of consecutive HSQC spectra (Bodenhausen and Ruben, 1980), using Sparky 3.114 (Goddard and Kneller). A single exponential decay function was fitted to the data to obtain the observed exchange rate, k_{ex}. In order to obtain the protection factors, PFs (*i.e.*: the ratio of the intrinsic and observed exchange rates of individual groups; k_{rc}/k_{ex}; Bai et al., 1993) of the assigned residues, k_{rc} (intrinsic exchange rates for totally denatured proteins) values were estimated based on the primary sequence, temperature and pH using the program SPHERE (http://www.fccc.edu/research/labs/roder/sphere). The conformational stability, ΔG_{HX} (**Figure S3**), of each HN group was calculated as:

$$\Delta G_{HX} = -RT\ln(k_{rc}/k_{ex}) = RT\ln PF.$$

In the case of (I27wt)$_8$, and although the exchange of the most protected HNs was incomplete under our experimental conditions (~2 days, pH 5.05, 25 ºC), the calculated PF values clearly show that the most protected residues are located in the secondary structures (β-strands) while HN in the loops and N- and C-termini exchange easily with the deuterated solvent. Interestingly, among these less protected regions, the N-terminus, residues 1-5 and 26-27, is the most stable, in accordance with the reported stabilizing effect of the nearby A78T mutation (**Figure 2F**; Stacklies et al., 2009). (I27Y9P)$_{12}$ showed lower conformational thermal stability (**Figure S4**) and the most protected regions were similar to those found in the wt form; they belong to interior H-bonding sites of β-strands. Besides, it seems that the N-terminal region of the protein (residues 1-9, 23, 26, 27, 74, 75 and 80) also shows the largest drop in protection, which would be in line with the perturbation in the mechanical intermediate suggested in the main text (**Figures 2D, E and H**).

SMFS

Before each SMFS experiment, the cantilever tip was cleaned for 1 min with a UV lamp (UV/Ozone ProCleaner™ Plus, Bioforce Nanosciences Inc.). The equipartition theorem (Florin, 1995) was used to calculate the spring constant of each cantilever with a Si_3N_4 tip (MLCT, Veeco Metrology Group; and Biolever, Olympus), which ranged from 35 to 70 pN/nm for MLCT-AUNM and was ~30 pN/nm for Biolever cantilevers. The substrate surface with the adsorbed protein sample was put in contact with the tip to pick up proteins by absorption and then withdrawn along the *z*-axis several hundred nm to stretch the proteins. Experiments were performed in the so-called length-clamp mode of SMFS (Carrión-Vázquez et al., 2006), at 0.8 nm/ms (for (I27wt)$_{12}$ and (I27 Y9P)$_{12}$) and 0.4 nm/ms both for ((I27wt)$_{12}$ and (I27 Y9P)$_{12}$) homopolyproteins as well as pFS-1+I27wt and pFS-1+I27Y9P heteropolyproteins. At least 3 experiments were performed for each protein and condition. All the data were analyzed using custom-made procedures in Igor Pro 6 (Wavemetrics). The mechanical properties of proteins were obtained by fitting the force-extension curves to the WLC model of polymer elasticity (Bustamante et al., 1994; Marko and Siggia, 1995):

$$F(x) = \frac{k_B T}{p}\left[\frac{1}{4\left(1 - x/L_C\right)^2} - \frac{1}{4} + \frac{x}{L_C}\right],$$

where F is the force, p is the persistence length, x is the end-to-end length, and L_c is the contour length of the stretched protein. L_c and p are the adjustable parameters. It should be noted that for SMFS (and in thermal stability measurements) an (I27wt)$_{12}$ construct (instead of the (I27wt)$_8$ construct used in

NMR experiments) was used to optimize the detection of the intermediate state as a deviation from the main WLC fitting (**Figure 3A**). As our NMR data indicated that the I27wt tertiary structure remains intact when inserted in a polyprotein and hence, we could use any polyprotein construction for mechanical purposes, we chose a longer polyprotein as it is reported that the unfolding intermediate species results in a gain in length of 6.6 Å per module, thus an increase which is proportional to the number of repeats (Marszalek et al., 1999). Data are reported as mean ± standard deviation. All histograms are normalized.

We have repeated the experiments with the same $(I27Y9P)_{12}$ and pFS+Y9P samples in two different laboratories and AFM set ups to confirm our SMFS data (**Figure S5**). In the laboratory of Prof. Víctor Muñoz, the experiments were performed in a PicoForce AFM equipped with a NanoScope IIIa Controller (Veeco Metrology Group), using MLCT cantilevers (Veeco Metrology Group), with a spring constant ranging from 40-50 pN/nm. Gold coverslips (Gold Arrandee™) and the same experimental conditions as those used in our laboratory were employed (namely PBS [pH 7.5] as experimental buffer and a pulling speed of 0.8 nm/ms and 0.4 nm/ms for $(I27\ Y9P)_{12}$ and pFS+I27 Y9P, respectively). Although the recordings obtained in this AFM contained higher noise levels due to an incomplete isolation, the data obtained were perfectly comparable to those described in the main text. Similar results were also obtained for these samples on a third AFM set up, in the laboratory of Prof. Andrés Oberhauser (data not shown).

The speed dependence of the F_u was done in an AFS apparatus (Luigs & Neumann) using the Olympus cantilevers with a nominal spring constant of 30 pN/nm. The measured spring constant was calculated using the method described above. The buffer and substrate were the same than those used above. The Monte Carlo simulations used were described elsewhere (Rief *et al.* 1998).

SMD

The GBSA approach used here for the SMD simulations was described elsewhere (Valbuena et al., 2009) although here the temperature was controlled using Langevin dynamics with 2 ps^{-1} as collision frequency. The SMD simulations were carried out imposing a restraint to both the N- and C-termini of the protein and increasing its length at a rate of 1 Å/ps with a constant restraint force of 5 kcal/mol·$Å^2$ (**Figure 5** and **Figure S6**). The pulling velocity of the simulations (1 Å/ ps) is about 10^8 times faster than the experimental pulling speed (0.4 nm/ ms = 4 Å/ ms $= 4 \cdot 10^{-9}$ Å / ps). Due to this difference in pulling velocities, the force values obtained in our simulations were considerably higher than those observed experimentally (**Figure 5B** and **Table 1**). All protein trajectories were visualized by VMD 1.8.6 using the structures atomic coordinates (Humphrey et al., 1996), and the N_t-C_t distance and hydrogen bond lengths (for the hydrogen bonds that constitute the mechanical clamp of the modules) were measured. We selected nitrogen and oxygen atoms that remained closer than 3.8 Å in most of the free molecular dynamics simulations, and the length of the selected backbone hydrogen bonds (with an angle cut off: < 35º) was monitored along the SMD. Forces were calculated from $C_{\alpha N\text{-}t}$-$C_{\alpha C\text{-}t}$ distance as follows:

$$F = -k\cdot[(N_t - C_t)_{measured} - (N_t - C_t)_{(0)} - v\cdot t].$$

Thermal denaturation

To assess the overall secondary structure of I27 (**Figure S4**), we monitored the I27wt, I27 Y9P, $(I27wt)_{12}$ and $(I27\ Y9P)_{12}$ far UV-CD spectra at 25 ºC in a JASCO-J810 spectropolarimeter (JASCO Inc.), equipped with a Peltier temperature control unit, using 1 mm-pathlength quartz cuvettes. The experimental buffer was 100 mM sodium phosphate/150 mM NaCl/1mM DTT [pH 7.5] and the protein concentration ranged 0.5-1 mg/ml.

The same instrument was used to monitor thermal denaturation experiments (**Figure S4**, **Table 1**). The heating rate was 0.5 ºC/min and the reversibility of the denaturation process was determined by comparing the spectra of the native proteins (before their thermally induced denaturation) with those obtained after rapidly re-cooling the heated samples. The observed changes in ellipticity (θ) at 229 nm wavelength were used to follow protein denaturation. The buffer contribution to (θ) measurements was substracted from the results that are shown. Molar ellipticity ($[\theta]$) was calculated as following (Bain et al., 2001):

$$[\theta] = \theta \cdot 100 \cdot Mr/c \cdot l \cdot Na,$$

where *Mr* is protein´s molecular weight (in Dalton), *c* is the protein concentration (in mg/ml), *l* is pathlength (in cm) and *Na* the number of residues – 1.

A model which assumes a two state folded ↔ unfolded equilibrium and linearly sloping pre- and post-transition baselines was fit to the data to obtain the parameters shown in **Table 1**.

Supplemental references

Bai, Y., Milne, J.S., Mayne, L., and Englander, S.W. (1993). Primary structure effects on peptide group hydrogen exchange. Proteins *17*, 75-86.

Bain, D.L., Berton, N., Ortega, M., Baran, J., Yang, Q., and Catalano, C.E. (2001). Biophysical characterization of the DNA binding domain of gpnu1, a viral DNA packaging protein. J. Biol. Chem. *276*, 20175-20181.

Bodenhausen, G., and Ruben, D.J. (1980). Natural abundance nitrogen-15 NMR by enhanced heteronuclear spectroscopy. J. Chem. Phys. Lett. *69*, 185-189.

Bruix, M., Ribó, M., Benito, A., Laurents, D.V., Rico, M., and Vilanova, M. (2008). Destabilizing mutations alter the hydrogen exchange mechanism in Ribonuclease A. Biophys. J. *94*, 2297-2305.

Florin, E.L., Rief, M., Lehmann, H., Ludwig, M., Dornmair, C., Moy, V.T., and Gaub, H.E. (1995). Sensing specific molecular interactions with the atomic force microscope. Biosens. Bioelectron. *10*, 895-901.

Geoghegan, K.F., Dixon, H.B., Rosner, P.J., Hoth, L.R., Lanzetti, A.J., Borzilleri, K.A., Marr, E.S., Pezzullo, L.H., Martin, L.B., LeMotte, P.K., McColl, A.S., Kamath, A.V., and Stroh, J.G. (1999). Spontaneous alpha-N-6-phosphogluconoylation of a "His tag" in Escherichia coli: the cause of extra mass of 258 or 178 Da in fusion proteins. Anal. Biochem. *267*, 169-184.

Hermans, J., Berendsen, H.J.C., Van Gunsteren, W.F., and Postma, J.R.M. (1984). A consistent empirical potential for water-protein interactions. Biopolymers *23*, 1513-1518.

Humphrey, W., Dalke, A., and Schulten, K. (1996). VMD: Visual Molecular Dynamics. J. Mol. Graph. *14*, 33-38.

Huyghues-Despointes, B.M., Pace, C.N., Englander, S.W., and Scholtz, J.M. (2001). Measuring the conformational stability of a protein by hydrogen exchange. Methods Mol. Biol. *168*, 69-92.

Krishna, M.M., Hoang, L., Lin, Y., and Englander, S.W. (2004). Hydrogen exchange methods to study protein folding. Methods *34*, 51-64.

Marley, J., Lu, M., and Bracken, C. (2001). A method for efficient isotopic labelling of recombinant proteins. J. Biomol. NMR *20*, 71-75.

Miroux, B., and Walker, J.E. (1996). Over-production of proteins in *Escherichia coli*: mutant hosts that allow synthesis of some membrane proteins and globular proteins at high levels. J. Mol. Biol. *260*, 289-298.

Rief, M., Gautel, M., Schemmel, A. and Gaub, H. (1998). The mechanical stability of immunoglobulin and fibronectin III domains in the muscle protein titin by atomic force microscopy. Biophys. J. *75*, 3008-3014.

Sambrook, J., Fritsch, E.F., and Maniatis, T. (1989). Molecular Cloning: A Laboratory Manual, 2nd Ed (New York: Cold Spring Harbor).